Analytical Modeling of Organic Light Emitting Diodes (OLEDs)

By

Apra Vyas

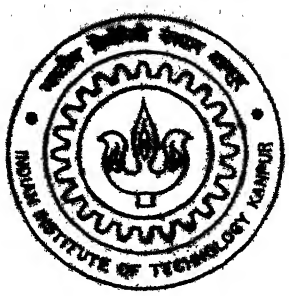

DEPARTMENT OF ELECTRICAL ENGINEERING

Indian Institute of Technology Kanpur

MARCH, 2003

Analytical Modeling of
Organic Light Emitting Diodes (OLEDs)

A Thesis Submitted
in Partial Fulfillment of the Requirements
for the Degree of

Master of Technology

By

Apra Vyas

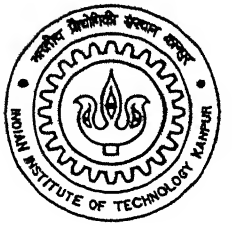

To the

DEPARTMENT OF ELECTRICAL ENGINEERING
INDIAN INSTITUTE OF TECHNOLOGY, KANPUR

March, 2003

CERTIFICATE

This is to certify that the work contained in the thesis titled **"Analytical Modeling of Organic Light Emitting Diodes (OLEDs)"** by Apra Vyas (Roll No. Y110408) has been done under my supervision and that this work has not been submitted elsewhere for a degree.

Dr. Baquer Mazhari
Associate Professor
Department of Electrical Engineering
Indian Institute of Technology
Kanpur-208016
India

March 2003

TO THE ALMIGHTY GOD

ACKNOWLEDMENTS

I take this opportunity to express my sincere gratitude to my thesis supervisor Dr. B. Mazhari without whose support I couldn't have completed this dissertation. I am especially thankful to him for his tolerance to my wayward writing and taking pains in reading and improving the dissertation and bringing it to its present form. I also sincerely acknowledge his support and guidance throughout the thesis.

I am thankful to mummy, papa and all the members of my family for their love and affection. I specially want to thank my dear mother, from whom my happiness begins, for giving me courage to follow my dreams and putting up with me during most stressful time. Special thanks to my dear brother Tinu for his encouragement, and the faith he bestowed in my ability.I would also like to thank my uncle Prof .Satish Purohit for his care and guidance throughout these years .

I am especially thankful to Dr Avinash Joshi for his kindness and invaluable guidance. I also want to thank Prof Jain and his family, Himani's Mother, Shubham Didi and Shivani for their support. Though they do not bear any direct relationship with my thesis work, but their concern and help during my stay in IITK made things easier for me.

I wish to thank Samtel for providing financial support. Lastly I would like to thank all the members of VLSI lab for their timely help and assistance.

Apra Vyas

ABSTRACT

Organic light-emitting devices (OLEDs) represent a promising solution for the flat-panel displays of the new generation. In an effort to study the fundamental science underlying their functioning, most of the studies so far have relied on numerical tools for analysis. However attempts made to study the device phenomenon with the help of numerical simulations obscure the underlying device operation. Study under analytical framework provides a deeper understanding into the device operation. The aim of present work is to develop analytical models for the bilayer devices in particular, which reveals the dependence of current, efficiency etc on various devices parameters. Analytical models developed for single carrier bilayer device adequately predict quantitative dependence of current voltage (J-V) characteristics on energy and mobility discontinuities at the organic interface. The current is predominantly interface barrier limited and dependence of the current on both the voltage and thickness is identical. The understanding gained from the single carrier devices is then applied to study bilayer devices under bipolar injection condition. Another important aspect of the present work is to explore the injection conditions analytically, when the developed models are likely to hold good.

CONTENTS

List of Symbols

Symbol	Description	Unit
k	Boltzmann constant	J/K
q	Charge	C
n	Electron concentration	cm^{-3}
p	Hole concentration	cm^{-3}
γ	Langevien recombination constant	sec
v	Carrier velocity	cm/s
$\varepsilon_o\varepsilon_r$	Permittivity	F/cm
χ	Electron Affinity	eV
ϕ_h	Hole Barrier	eV
ϕ_n	Electron Barrier	eV
μ_p	Hole Mobility	cm^2/V-sec
μ_n	Electron Mobility	cm^2/V-sec
J	Current Density	A/cm^2
J_p	Hole Current Density	A/cm^2
J_n	Electron Current Density	A/cm^2
E	Electric Field	V/cm
E_v	Valence-band energy	eV
E_c	Conduction-band energy	eV
ΔE_v	Offset between valence-band	eV
ΔE_c	Offset between conduction-band	eV
V	Applied bias	V
V_{bi}	Built-in voltage	V

U	Recombination density	cm^{-3}
C	Capacitance	F
T	Temperature	K
A	Richardson's constant	$A/cm^2/K^2$

List of figures

List of tables

Chapter 1

Introduction

The observation of efficient electro-luminescence in organic semiconductors a decade ago added a new dimension to conventional display technology. Prospects for low manufacturing cost, ease of processing, color range and mechanical flexibility make them appealing candidates as active material in light emitting diodes (LEDs). Besides efficiencies, brightnesses and low drive voltages already achieved have established that their use in display applications is a real possibility [1].

The simplest organic light emitting diode structure consists of a thin layer of conjugated (alternate single and double bond) luminescent organic material sandwiched between two metal contacts .The organic materials used in OLEDs are undoped and have negligible intrinsic carrier densities, so that the current flow is due to charge carriers injected from the contacts. Adding an electronic charge to the undoped organic layer creates an accompanying lattice deformation. The charge and the accompanying lattice deformation is called as a *polaron*. For convenience, electron polarons and hole polarons are referred to simply as electrons and holes [2].

The rectification and light-emitting properties of the organic LED are caused by the use of asymmetric metal contacts. High work function metals inject holes more efficiently than electrons, and similarly low work function metals inject electrons more efficiently than holes. Therefore the high work function metal act as anode and the low

work function metal act as cathode. This also defines the forward and reverse bias directions of the diode [3]. When sufficiently large bias is applied across the contacts, then the electron polarons are injected from one contact and the hole polarons are injected from the other contact. Polarons move across the device under the influence of electric field, until two charges of opposite polarity encounter each other, and recombine to form an exciton. Either a singlet or triplet exciton can be formed when an electron or hole annihilate together. The branching ratio for forming singlet or triplet excitons is not known, but if it is governed by statistics alone, then three triplets would be formed for every singlet. Since only the singlet excitons have an allowed optical transition to the ground state, therefore existence of triplet excitons would reduce possible organic LED efficiency by a factor of four [4].

Although easy to fabricate, such single layer organic LEDs are often inefficient. Two principal factors that limit the efficiency of single layer organic LEDs are: (i) different electron and hole mobilities cause the recombination to occur near a metal contact where dipole quenching and nonradiative losses reduce device efficiency, and (ii) unbalanced carrier injection results in a large fraction of one carrier type traversing the device without recombining. Bilayer, heterojunction organic LEDs are able to address these problems by controlling the distribution of carriers in the device using discontinuities in either the energy levels or carrier mobilities of the two organic materials used to fabricate the device. When the mobilities of the electrons and holes are significantly different, but good contacts can be made for both carrier types, then the role of the bilayer structure is to move the recombination away from the electrode that injects low mobility carrier. In an organic material having equal electron and hole mobilities, but where the electron-injecting contact is not able to supply electrons fast enough to recombine with all the easily injected holes, the role of bilayer structure is to prevent the holes from traversing the device without recombining. Use of energy level discontinuities to block the transport of the carrier that has higher mobility or that is injected more favorably, increases the device quantum efficiency. However, the device power efficiency, which is usually an important metric for LED performance, decreases. This requirement of large drive voltage can be remedied either by making the blocking layer

thinner or, by employing a layer that blocks the transport of favorable carrier and also enhances the qualities lacking in the inferior carrier [5].

Electro-luminescence in these multilayer devices is controlled by the buildup of internal space charges, across the organic interface. Low charge-carrier mobilities lead to the space charge buildup. Furthermore, presence of energy level offsets at the organic material interface in a hetero or multilayer device can be an additional source of buildup of interfacial space charges. Even in the absence of these energy barriers, the abrupt differences of charge-carrier mobilities in the respective layers of typical multilayer devices, lead in effect to the presence of mobility barriers at the hetero-interfaces, which in turn can be the source of interfacial space-charge formation. The interfacial charges have significant impact on the electro-luminescence and the performance of organic light-emitting diodes (OLEDs). Results clearly demonstrate that the tailoring of internal barriers in multilayer devices leads to significant improvement in device performance [6].

OLEDs are a relatively new type of device. Because of this, the fundamental science underlying their functioning is still largely unexplored or poorly understood, and this may ultimately constitute an inhibiting factor for progress in the development of better-performing devices. Although considerable progress has been made in understanding the underlying science and solving issues that limit device performance, the operation of OLED, in particular multilayer devices, is still not fully understood. Most of the studies reported so far have employed numerical simulations as a tool for device analysis [6-8]. Although these simulations provide precise quantitative results, they often do not lead to a deeper understanding of the device itself. Analytical models, although comparatively less accurate, have the advantage that they offer better insight into the device operation. However, because of the complexity of carrier injection, transport and recombination, very few analytical models have been reported. Even those that have been attempted end up with a set of transdental equations that has to be eventually solved by a computer [7]. A closed form expression revealing the dependence of current, efficiency etc on the device parameters is lacking at present. The aim of the present thesis is to develop such models for bilayer devices.

This thesis is organized in five chapters. In chapter-2 analytical models for the current-voltage characteristics (*J-V*) of single carrier bilayer structure both in the forward and reverse direction have been obtained. Chapter-3 is devoted to obtain analytical model for current-voltage characteristics (J-*V*) under bipolar injection condition and study of recombination for efficient luminescence. One simplifying assumption that is made during development of these analytical models is that the current is bulk-limited. Chapter-4 is devoted to the examination of conditions, under which this condition is likely to be true. Finally in chapter-5 the thesis concludes with important results of the present work.

Chapter 2

Single carrier hole only Bilayer device

2.1:Introduction: Carriers injected into the organic layer can either recombine in the film or they can traverse the structure and reach the other contact without recombining. Carriers that traverse the device without recombining are wasted and the structure must be designed to minimize this possibility. Since the selection of electrode material and active components on the premise of their work function as well as their oxidation and reduction potentials is limited, one has to resort to more elaborate strategies, not only to improve injection, but at the same time to make optimum use of carriers once injected. Bilayer diodes employing two organic layers with different electronic energy structure and different charge carrier mobilities, allow these criteria to be more readily satisfied.

Bilayer structures make use of two layers of different organic material. At the interface between two organic layers there is sizeable offset in energies of the HOMO and/or LUMO level of two layers [7]. Organic material which transports holes efficiently is referred to as hole transport layer (HTL), and one which blocks passage of holes is referred to as hole blocking layer (HBL) as shown in Fig.2.1. Offset at the interface, impedes the passage of carriers across the LED. This results in internal charge accumulation, redistribution of electric field, and associated feedback effects concerning the injection of holes and electrons, as well as branching between the recombination and drift towards the contacts [7,8]. Thus the relative energy levels and mobilities of electrons and holes of organic materials are important device design parameters, which play an important role in the operation of the device.

To provide a framework for understanding bilayer devices, the effect of energy level discontinuities at organic heterojunction are first studied in a bilayer single carrier (hole-only) structure. We develop analytical models that describe current density-voltage characteristics of bilayer hole-only device in the forward as well as reverse direction. These models explain the effect of hole energy level discontinuity on the current-voltage characteristics, and provide insight into operation of the device.

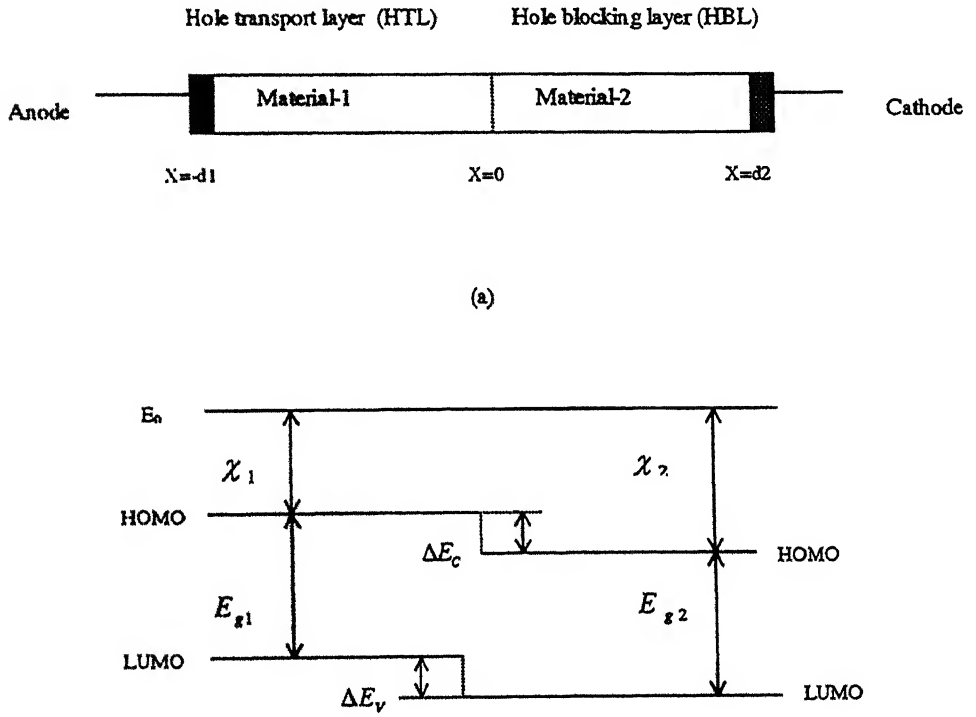

Fig.2.1 (a) Schematic diagram of a bilayer organic LED (b) and its associated energy band diagram.

2.2:Analytical Model: Forward bias:

We consider a bilayer organic device structure with material parameters typical of the conjugate organic materials used in OLEDs. The basic structure of an OLED consists of

metal/material-1/material-2/metal, where material-1 act as hole-transport layer (HTL), and material-2 act as hole-blocking layer. Fig.2.1 shows structure of bilayer device with the associated band diagram. For sake of simplicity, we assume that the conduction energy level E_c is same for both the organic materials, and there is only a 'valence-band' discontinuity at the organic interface. The hole injection barrier at the left contact is small (0.2eV), and electron injection barrier at the right contact is large enough to essentially make it a hole-only device.

The interface is assumed to be free of sheets of charge, dipoles, or recombination, so that there is continuity of the electric displacement D, and the electrostatic potential ϕ across the interface. During initial analysis, the hole mobility is assumed to be constant and same in both the materials. Both the materials are assumed to have the same dielectric constant and the transport of holes in both the materials is assumed to be trap-free. The analytical model assumes drift-diffusion transport in the bulk and thermionic emission at metal-organic interface. It is well known that under bulk-limited and trap-free condition, the current in a single layer hole-only device is described by space charge limited current (SCLC) flow:

$$J = \frac{9}{8}\varepsilon_0\varepsilon_r\mu_p(V^2/d^3) \qquad (2.2.1)$$

where the symbols have their usual meaning. The presence of 'valence-band' discontinuity of height ΔE_v might be expected to reduce SCLC current in a hole-only bilayer device by a factor of $\exp(-\Delta E_v/kT)$ so that the current density is given as:

$$J = \frac{9}{8}\varepsilon_0\varepsilon_r\mu_p(V^2/d^3)\times\exp(-\Delta E_v/kT) \qquad (2.2.2)$$

In order to investigate the validity of this simple picture, numerical simulations were carried out using SimWindows simulator [17], which is based on drift-diffusion formalism in the bulk and thermionic emission at the metal-organic interface. Fig.2.2

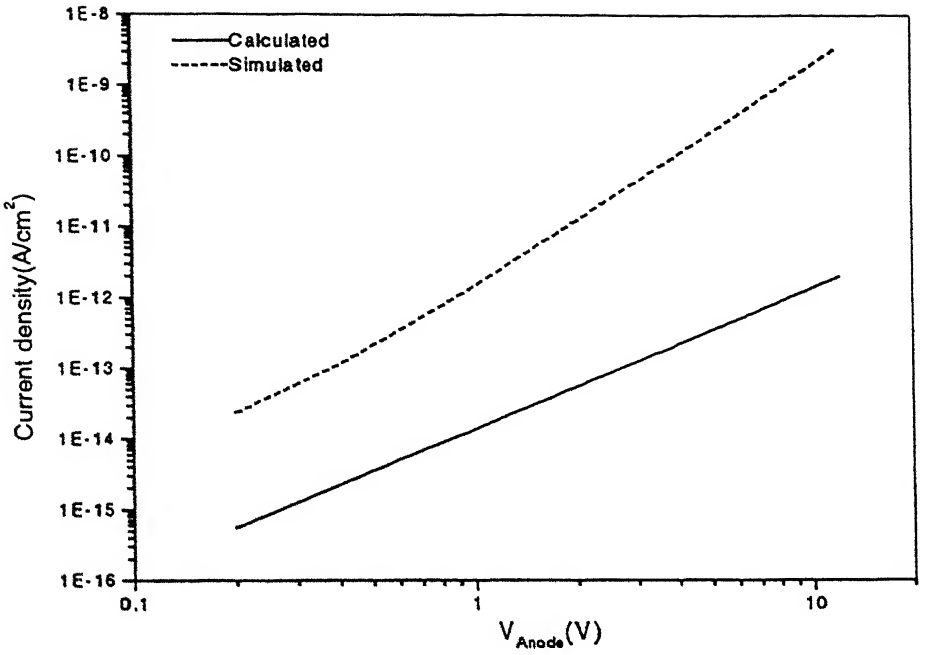

Fig.2.2 Current density as a function of applied bias obtained from numerical simulations (dotted line) of device shown in Fig.2.1 and that obtained from Eq.2.2.2 (solid line). The electron affinity is 3.0eV for both the organic materials. The band gap for organic material-1 is 2.4eV, and for organic material-2 is 3.0eV. The organic layers are each 500A° thick and have the same hole mobility μ_h as 0.5×10^{-6} cm^2/V-sec.

shows comparison of the result in a hole-only bilayer device obtained with the help of numerical simulations and those predicted by Eq (2.2.2), under forward bias condition .It can be seen that not only is the magnitude of the current predicted by the simple picture an underestimation of value obtained by numerical simulation, but the slope of the curve is also larger than 2, indicating that the current density can no longer be modeled as space charge limited. Although simulations do indicate that the current scales as $\sim\exp(-\Delta E_v/kT)$, *It is clear that barrier at the organic interface plays a more complex role.*

Fig 2.3a and Fig 2.3b shows spatial variation of the hole density and the electric field as a function of 'valence-band' discontinuity at the organic interface. The simulation results

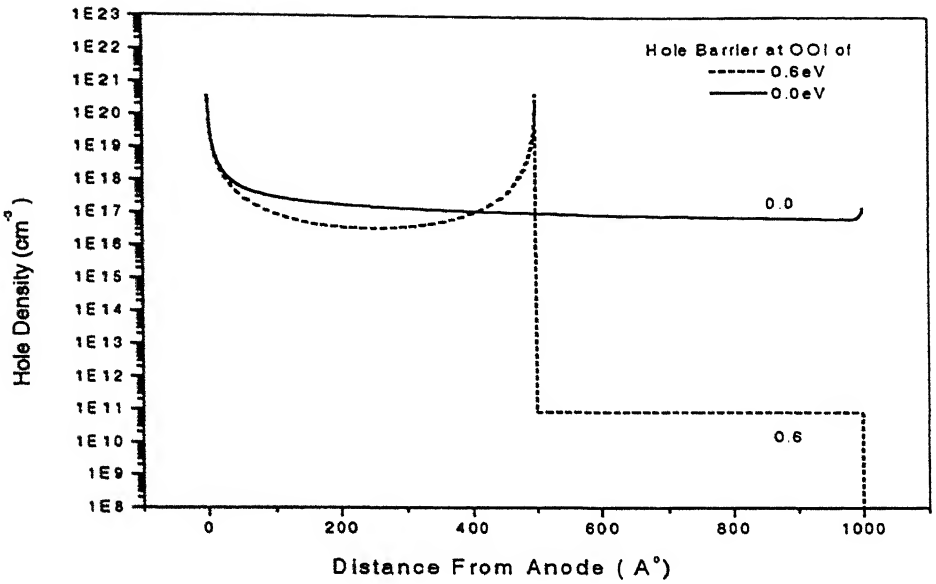

Fig.2.3b Simulated variation of hole density profile for bilayer hole only devices as shown in Fig. 2.1 as a function of hole energy level discontinuity at the organic interface, at an applied bias of 12V. The electron affinity is 3.0eV for both the organic materials. The band gap for organic material-1 is 2.4eV, and for organic material-2 is varied from 2.4eV to 3.0eV. The organic layers are each 500A° thick and have the same hole mobility μ_h as 0.5×10^{-6} cm^2/V-sec.

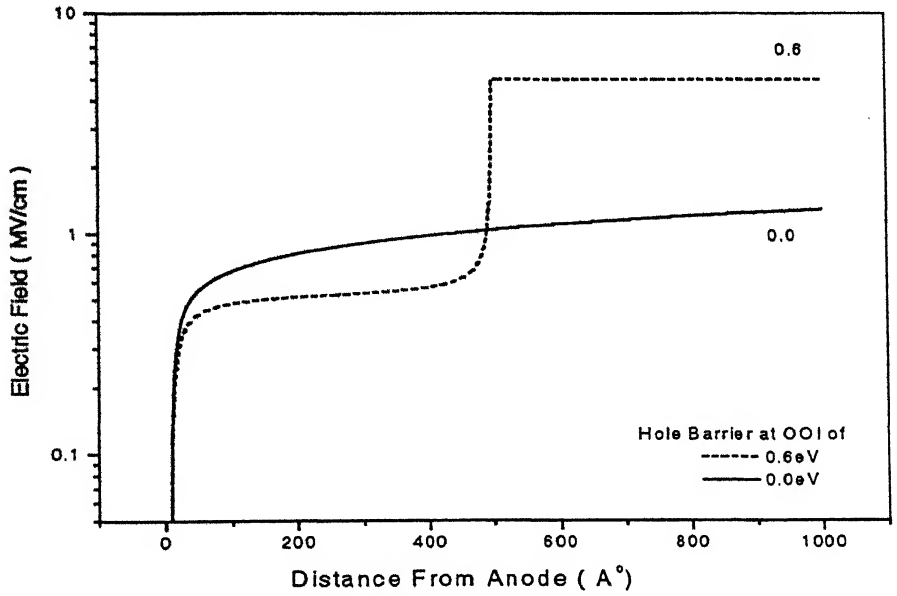

Fig.2.3b Simulated variation of electric field profile for the hole only as shown in Fig. 2.1 bilayer devices as a function of hole energy level discontinuity at the organic interface, at an applied bias of 12V. The electron affinity is 3.0eV for both the organic materials. The band gap for organic material-1 is 2.4eV, and for organic material-2 is varied from 2.4eV to 3.0eV. The organic layers are each 500A° thick and have the same hole mobility μ_h as 0.5×10^{-6} cm^2/V-sec.

show, that for large hole barrier at the organic interface, hole density to the left of interface, $p(0^-)$ is much larger than the hole density to the right of interface $p(0^+)$. Spike in the hole density to the left of organic interface causes rapid change in the electric field at the interface. Thus, field in the hole blocking layer (HBL) is significantly larger than the field in the hole transport layer (HTL). For a large barrier of 0.6eV at the organic interface, almost all the electric field lies in the hole blocking layer (HBL). The electric field in the blocking layer is almost independent of the position, and increases rapidly with 'valence-band' discontinuity at the organic interface. This is in contrast to the electric field in the transport layer, where field is small and increases slowly with the 'valence-band' discontinuity.

Thus addition of blocking layer has two important effects, it results in accumulation of charges in the vicinity of organic interface by impeding the flow of carriers, and because of charge accumulation there is redistribution of electric field in the structure. This accumulation of holes at the interface tends to offset the tendency of the barrier to reduce carrier injection thereby resulting in larger current values.

In the absence of any dipole layer at the interface, the electric field would be continuous across the interface so that drift component of hole current to the left of the interface ($J_p^{drift}(0^-)$) would be much larger than drift component of hole current to the right of the interface ($J_p^{drift}(0^+)$). The only way in which continuity of hole current across the interface can then be maintained is if there is a large component of hole diffusion current to the left of the interface which is practically equal and opposite to the hole drift current.

$$J_P^{Drift}(0^-) \cong -J_P^{Diff}(0-) \qquad (2.2.3)$$

The presence of diffusion current, which opposes the drift current, implies positive gradient in hole concentration and thus accumulation of holes at the interface. Eq (2.2.3) also implies that quasi-equilibrium can be assumed to exist immediately to the left of the

organic interface, an important result that would be found very useful later in the derivation of the analytical model.

From the Fig2.3b, it can be assumed without much error that the entire voltage across the device is dropped across the hole-blocking layer:

$$E(x \geq 0) \cong (V - V_{bi})/d_2 \qquad (2.2.4)$$

where V is the applied bias and V_{bi} is the built-in voltage. With the help of this expression, hole current in the hole-blocking layer can be expressed as:

$$J_p = qp(0^+)\mu_p \times (V - V_{bi})/d_2 \qquad (2.2.5)$$

The hole concentration in the vicinity of organic interface can be related to the hole barrier of height ΔE_v by:

$$p(0^+) = p(0^-) \times \exp(-\Delta E_v / kT) \qquad (2.2.6)$$

As it is clear from the simulation results that the presence of the barrier results in large accumulation of holes at the left side of interface. If we assume, $(p(x) << p(0^-)$ for $x < 0^-)$ i.e. hole density elsewhere in the hole transport layer can be neglected in comparison with the hole density at the interface (Q_p), then application of Gauss's law at the interface gives:

$$Q_p \cong \varepsilon_0 \varepsilon_r \times (V - V_{bi})/d_2 \qquad (2.2.7)$$

The simulation results also show that the hole density decays rapidly away from the interface in hole transport layer (HTL) which we assume to be exponential in nature:

$$p(x) = p(0^-) \times \exp(\delta x) \qquad \text{for } (x<0) \tag{2.2.8}$$

Integration of Eq. (2.2.8) and substitution in Eq. (2.2.7) gives:

$$p(0^-) = (\varepsilon_0 \varepsilon_r / q) \times \delta \times (V - V_{bi})/d_2 \tag{2.2.9}$$

Eq. (2.2.8) together with Eq. (2.2.3) implies quasi-equilibrium at the organic interface and yields an expression relating electric field at the interface and parameter δ :

$$E(0^-) = (kT/q) \times \delta \tag{2.2.10}$$

Eq. (2.2.9), Eq. (2.2.10) along with Eq. (2.2.4) provides means of relating $p(0^-)$ with the applied voltage as:

$$p(0^-) = (\varepsilon_0 \varepsilon_r / kT) \times ((V - V_{bi})/d_2)^2 \tag{2.2.11}$$

Substituting Eq. (2.2.11) and Eq. (2.2.6) in Eq. (2.2.5) we arrive at the central expression for current density:

$$J_p = \varepsilon_0 \varepsilon_r \times \mu_p \times \frac{q}{kT} \times (V - V_{bi}/d_2)^3 \times \exp(-\Delta E_V / kT) \tag{2.2.12}$$

But Eq. (2.2.12) is valid only for interface barriers, which are large enough to justify the assumptions made during the derivation. As the barrier reduces in the limit $\Delta E_V \rightarrow 0$, the current predicted by Eq. (2.2.12) does not go to the SCLC limit. This drawback can be rectified by casting Eq. (2.2.12) in a more instructive form as:

$$J_p = \left(\frac{9}{8} \varepsilon_0 \varepsilon_r \mu_p \frac{(V - V_{bi})^2}{d^3} \right) \times \exp(-\Delta E_V / kT) \times \left(\frac{8}{9} \times (\frac{d}{d_2})^3 \times \frac{V - V_{bi}}{kT/q} \right) \tag{2.2.13}$$

While the first term describes the conventional space charge limited current, the second term describes the role of the barrier in reducing carrier injection into the hole-blocking layer. The last term can be looked upon as the effect of barrier in causing accumulation of holes at the interface. A direct consequence of Eq. (2.2.13) is a new expression, which would correctly predict the behavior from large interface barriers down to zero interface barrier as well:

$$J_p = \frac{\frac{9}{8}\times\varepsilon_0\varepsilon_r\times\mu_p\frac{(V-V_{bi})^2}{d^3}}{1+\exp(\Delta E_v/kT)\Big/\frac{8}{9}\times(\frac{d}{d_2})^3\times(\frac{V-V_{bi}}{kT/q})} \qquad (2.2.14)$$

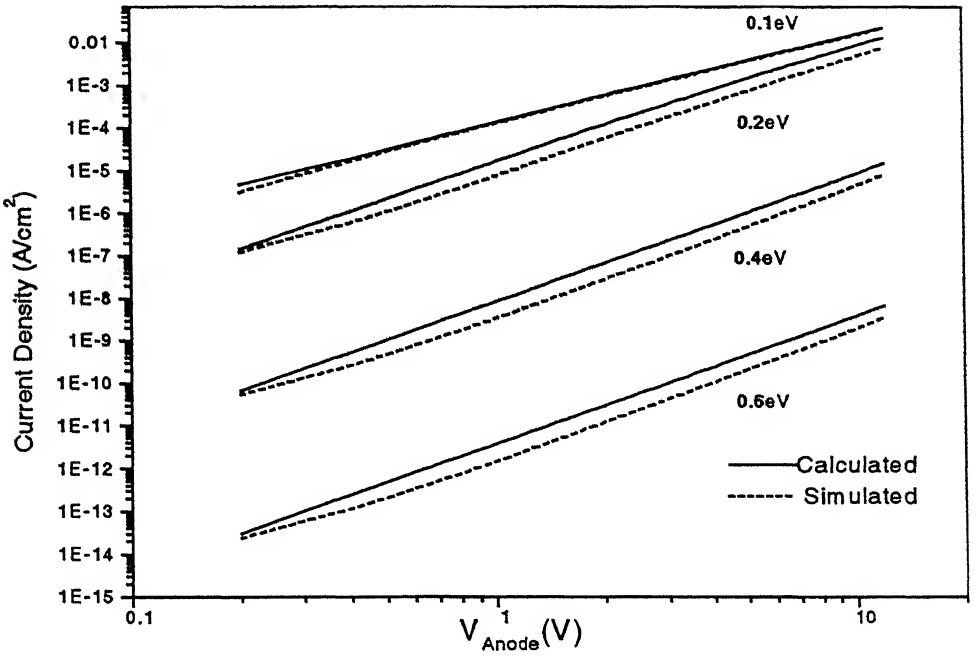

Fig2.4 Current density as a function of applied bias obtained from numerical simulation (dotted lines) and that obtained from Eq. (2.2.14) (solid lines) for the hole-only bilayer device as a function of different values of hole barrier height ΔE_V at the organic interface. The hole mobility is equal to 0.5×10^{-6} cm^2/V-sec in both the layers. The electron affinity is 3.0eV for both the organic materials. The band gap for organic material-1 is 2.4eV, and for organic material-2 is varied from 2.5eV to 3.0eV.

2.4:Results and discussion: Fig 2.4 shows that the current values predicted by the above expression matches very well with the simulation results for the barrier heights varying from 0.6eV down to 0.1eV. Figure shows, variation of current density as the cube of applied voltage $\sim (V - V_{bi})^3$, and inverse cube of the blocking layer thickness i.e. $\sim 1/d_2^3$. Eq. (2.2.14) reduces to Eq. (2.2.12) for the interface barriers that are larger than about 0.25eV. In this case the current is predominantly interface barrier limited and dependence of the current on both the voltage and thickness is identical. However the proposed model slightly overestimates the current. This is because of two assumptions made during the derivation; first it was assumed that the entire voltage drops across the hole-blocking layer, which results in overestimation of field in this region. Secondly, it was assumed that hole density elsewhere in HTL, is small compared to that at the interface, which results in overestimation of hole density at the interface.

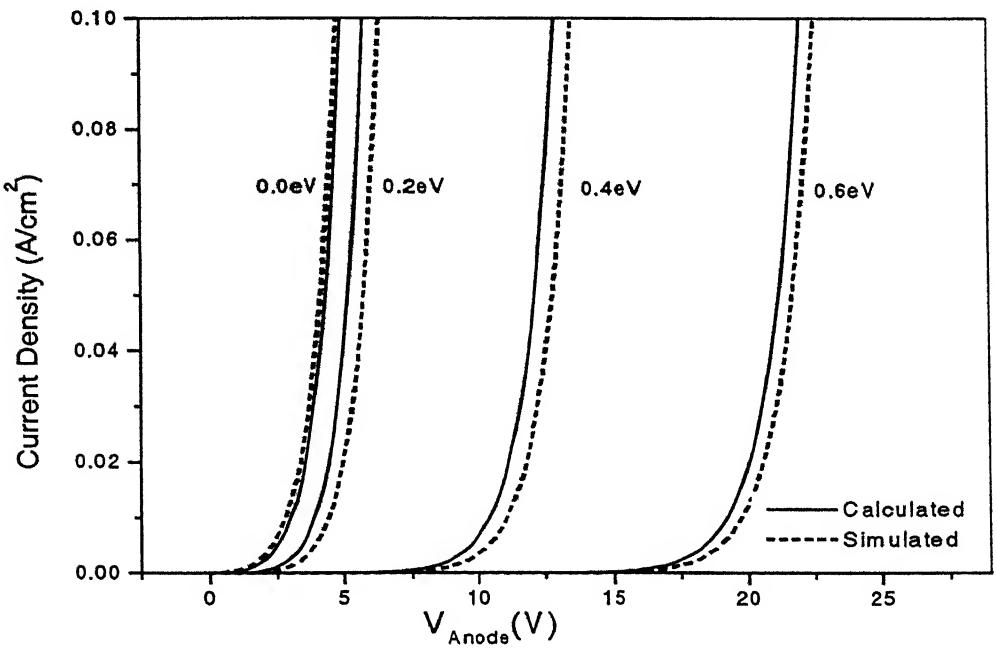

Fig.2.5 Current-Voltage (J-V) characteristics for hole-only bilayer device, as a function of valence band discontinuity, taking into account field dependence of hole mobility. Curves show increase in the voltage to attain the same value of current density of 0.1A/cm^2. Curves are obtained with reference to Eq. (2.2.15) with similar device parameters as used to obtain Fig.2.4.Value of E_0 is nearly equal to 1.5×10^4 V/cm and hole mobility μ_h is 0.5×10^{-6} cm^2/V-sec in both the layers.

For large hole barrier heights, it is easy to incorporate the dependence of mobility on the electric field since the field in the hole-blocking layer is large and uniform. Assuming $\mu_{p2} = \mu_{02} \times \exp\left(\sqrt{E/E_0}\right)$, we obtain a more general expression for current density in a hole-only bilayer device for large hole interface barrier heights as:

$$J_p = \varepsilon_0 \varepsilon_r \mu_{02} \times \frac{q}{kT} \times \left(\frac{V - V_{bi}}{d_2}\right)^3 \times \exp\left(\sqrt{\frac{(V - V_{bi}/d_2)}{E_o}}\right) \times \exp(-\Lambda E_v / kT) \qquad (2.2.15)$$

Fig 2.5 shows that successively higher voltages are required to obtain the same value of current density as the energy barrier to hole injection from material-1 to material-2 is increased. Even the modest 0.2eV barrier causes an increase in the voltage required to

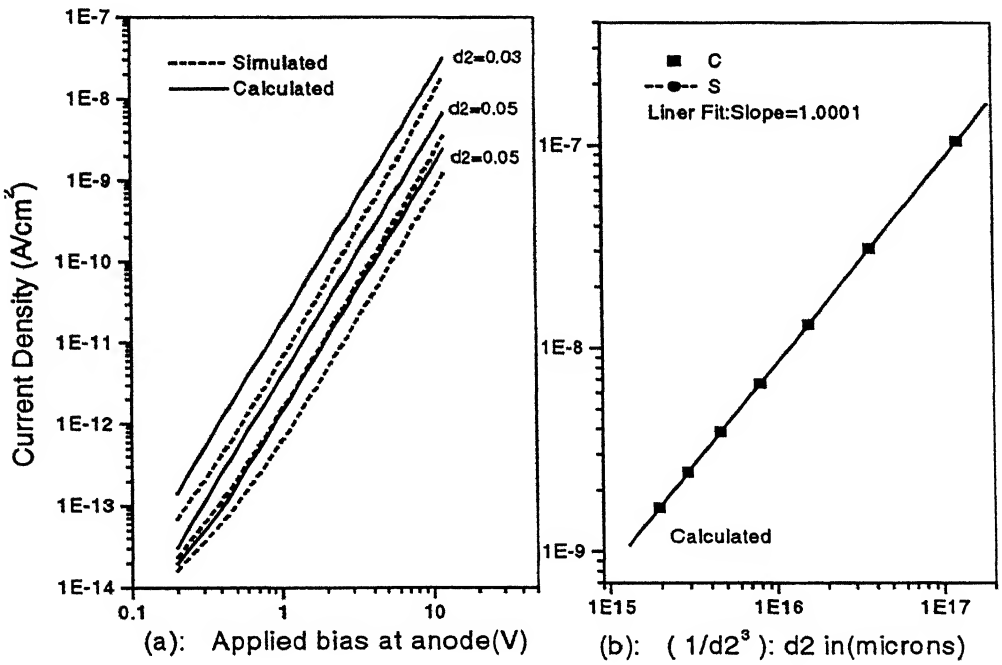

Fig.2.6a Calculated and simulated current density-Voltage characteristics for a bilayer hole only device with different blocking layer thicknesses. Solid lines are obtained from Eq. (2.2.14) and dotted lines are obtained from numerical simulation.**Fig.2.6b** Variation in current density w.r.t. variation in inverse cube of blocking layer thickness. Hole mobility μ_h is same 0.5×10^{-6} cm^2/V-sec in both the layers. In all the cases hole energy barrier at the organic interface is 0.6eV and electron energy barrier is 0.0eV.

obtain a given current. The curves are obtained by taking field dependence of mobility on the basis of Eq. (2.2.15). Similar results are reported by B.K. Crone *et. al* [5], but with E_o equal to $2\times10^4 V/cm$. At the larger values of hole barrier at the organic interface, current at a particular voltage is significantly reduced. It is evident that even a small increase in the barrier at the organic interface can significantly increase the biasing requirements. This increase in the voltage caused by the increase of barrier at organic-organic interface is different from what occurs at an energy barrier between a metal contact and an organic. For injection from a contact, the metal acts as a large reservoir of charge and the current is space charge limited. While in case of heterojunction barrier at organic interface, increase in the voltage required to achieve a given current density indicates significant impedance of hole transport layer.

Fig 2.6a shows the current density-voltage characteristics obtained for different values of blocking layer thicknesses, for the hole barrier height of 0.6eV at the organic interface. $d_2 = 0.03, d_2 = 0.05, d_2 = 0.07$ refers to the blocking layer thicknesses in microns for three different bilayer device structures. Fig.2.6b shows the variation of current density w.r.t variation of inverse cube of blocking layer thickness. Fig2.6a and Fig2.6b confirms that the current scales as $\sim 1/d_2^3$, which is in agreement with what is predicted by the developed analytical model.

The whole derivation was made under the assumption, that both the materials are same i.e. have same hole and electron mobility. Difference in the hole mobility also results in the accumulation of holes at the organic interface, and the impact of hole mobility discontinuity is similar to that of valence-band discontinuity. However an analysis of the steps involved in the derivation of analytical expression show that as long as there is a large accumulation of holes at the interface, the hole mobility difference in the two layers will not matter. Thus Eq. (2.2.12) will continue to hold good as long as barrier at the organic interface is large, except that μ_p has to be interpreted as μ_{p2}: mobility of the hole blocking layer. But as $\sim\Delta E_v \rightarrow 0$, Eq. (2.2.14) becomes equal to Eq. (2.2.1) for

SCLC in single layer single carrier device and the mobility should be interpreted as μ_{p1}. Though it is difficult to develop a general analytical model that is valid for arbitrary values of hole barrier heights and mobility ratios, but Eq. (2.2.14) can be modified to take into account different hole mobility values in the two organic layers both at large and small barrier height at the organic interface as well:

$$J_p = \frac{\frac{9}{8}\times\varepsilon_0\varepsilon_r\times\mu_{p1}\frac{(V-V_{bi})^2}{d^3}}{1+\frac{\mu_{p1}}{\mu_{p2}}\times\exp(\Delta E_v/kT)\Big/\frac{8}{9}\times(\frac{d}{d_2})^3\times(\frac{V-V_{bi}}{kT/q})} \qquad (2.2.16)$$

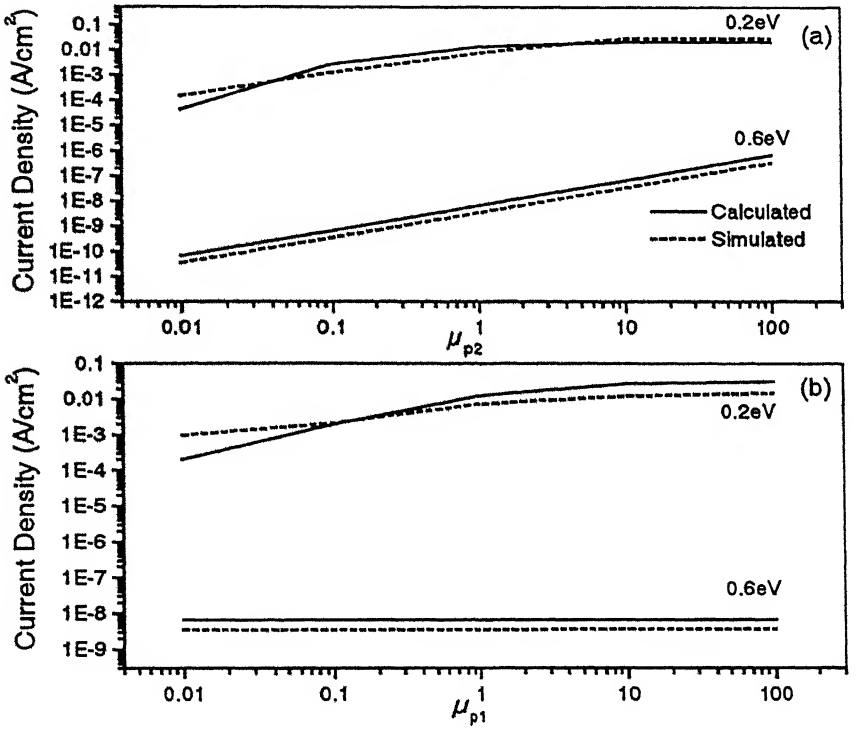

Fig 2.7 Shows variation in the calculated and simulated current density as a function of the transport and blocking layer hole mobility ratio μ_{p1}/μ_{p2}. In Fig.2.7 (a) blocking layer mobility μ_{p2}, is varied and in Fig.2.7 (b) transport layer mobility μ_{p1}, is varied. Calculated values (solid lines) are obtained from Eq. (2.2.16) and simulated values (dotted lines) are obtained from numerical simulation. In each case constant mobility has a value as 0.5×10^{-6} cm^2/V-sec, and hole barrier is 0.6eV(0.2eV) at the organic interface.

Fig 2.7 shows the dependence of current density on the mobility ratio for both large and small barrier heights. Fig 2.7a shows the current density plotted w.r.t variation in mobility ratio, when μ_{p1} (transport layer mobility) is kept constant and mobility of blocking layer, μ_{p2} is varied. While Fig. 2.7b shows variation of current density w.r.t variation in mobility ratio, when μ_{p1} is varied and μ_{p2} is kept constant. Both the figures along with equation establishes the fact that the current density is rather insensitive to the transport layer mobility, and scales directly with the blocking layer mobility, as long as barrier at the interface is kept large enough to block the transport of holes.

2.4:Analytical Model: Reverse bias:

In the previous section, an analytical model for bilayer hole-only device, under forward bias condition was developed. We further investigate the behavior of bilayer hole-only device under reverse biased condition. In this section the term reverse bias is used to define the condition when positive voltage is applied at cathode, and the injected carriers move from cathode towards anode, under the influence of electric field. This is different from the terminology used in normal semiconductor rectifying diodes, were such biasing condition significantly reduces the current carried by the diode. Here under the reverse bias condition barrier to hole injection at the cathode is low and current carried by the device is considerable.

Fig.2.8 shows the simulated electric field and hole density profile, for the hole-only two layer devices under reverse bias condition, for three different cases: (i) When the hole mobility in the transport layer is greater than the hole mobility in the blocking-layer (ii) When the hole mobility in the transport layer is less than the hole mobility in the blocking-layer (iii) When the hole mobility in the transport layer is equal to the hole mobility in the blocking-layer. These simulated results will aid in subsequent discussion, and the development of analytical models under reverse biased condition.

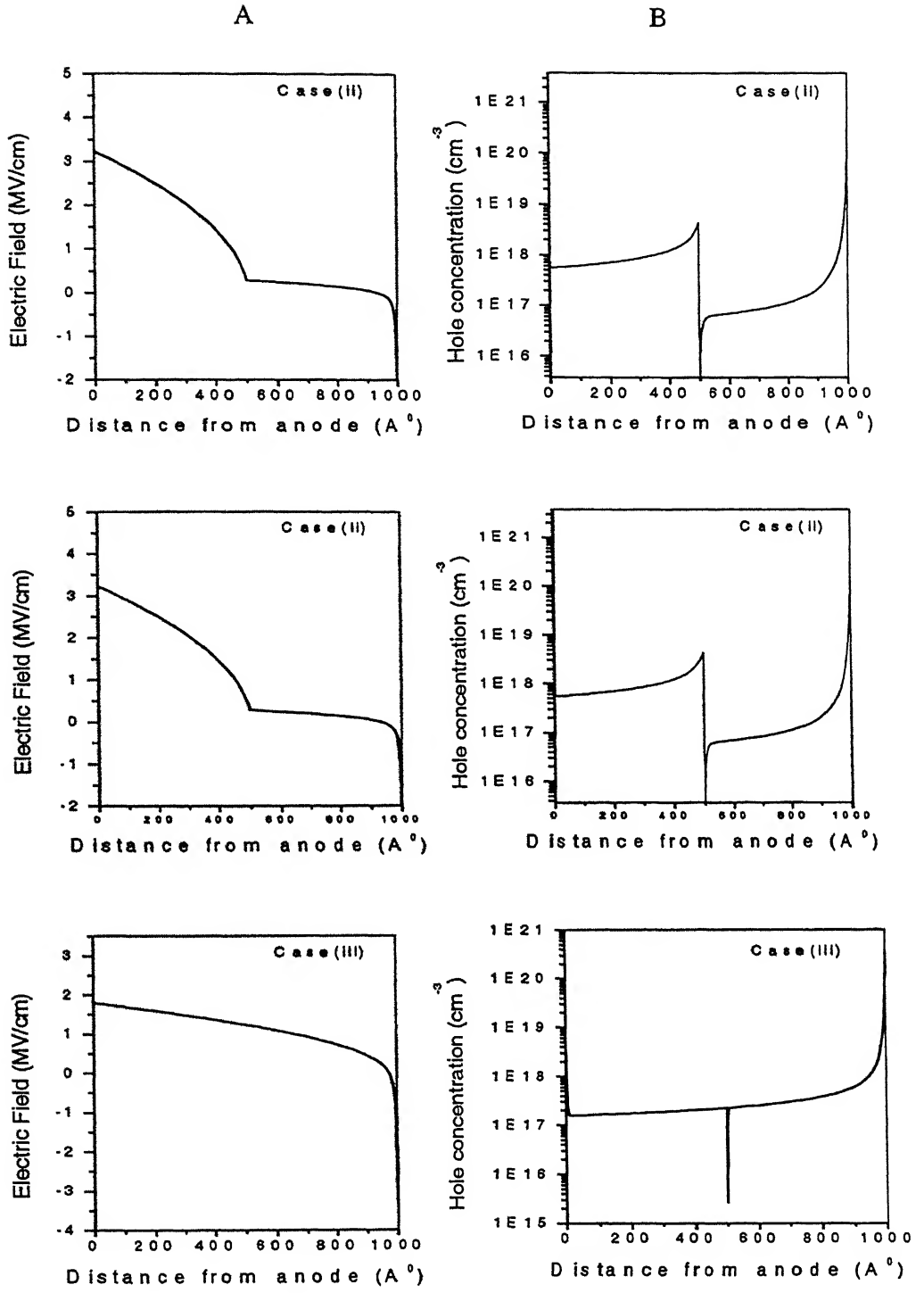

Fig.2.8a Shows simulated variation of electric field profile and. **Fig2.8b** shows simulated variation of hole density profile in a bilayer hole only device under the reverse bias condition. Ratio of hole mobility in the transport layer and in the blocking layer: μ_{p1}/μ_{p2} in case (i) is 100, in case (ii) is 0.01, and in case (iii) is 1.The hole mobility in the blocking layer in each case is 0.5×10^{-6}cm^2/V-sec.and hole injection barrier at the cathode is 0.2eV.The hole barrier at the organic interface is 0.6eV.

2.4.1 Case (i) $\mu_{p1} > \mu_{p2}$

The simulation results show, that the spatial variation of the electric field and charge density in the blocking-layer are similar to that of a single carrier (hole-only) single layer device. For small values of hole energy barrier at cathode, current in the blocking layer can be expressed under the limit of space charge limited conduction as:

$$J = \frac{9}{8}\varepsilon_o \varepsilon_r \mu_{p2} \frac{V_2^2}{d_2^3} \qquad (2.4.1.1)$$

where V_2 is the voltage drop across the blocking layer. If V_2 can be expressed as a function of applied voltage, then the current density can be determined in terms of known parameters. Thus the problem condenses to finding the fraction of applied voltage that drops across the blocking layer.

For the space charge limited conduction, spatial variation of electric field in the blocking layer can be expressed as [16]:

$$E(x) = \sqrt{\frac{2J(d_2 - x)}{\varepsilon_o \varepsilon_r \mu_{p2}}} \qquad (2.4.1.2)$$

Then the electric field at the organic interface $E(0)$, or at the distance d_2 from hole injecting contact becomes equal to:

$$E(0^-) = \sqrt{\frac{2Jd_2}{\varepsilon_o \varepsilon_r \mu_{p2}}} \qquad (2.4.1.3)$$

In the absence of dipole layer, electric field should be continuous across the organic interface:

$$E(0^-) \sim E(-d_1) \qquad (2.4.1.4)$$

The simulation results in Fig 2.8a show that the electric field is constant in the transport layer due to higher mobility of holes in the transport layer. Then the voltage drop across the blocking layer can be expressed as:

$$V_2 = V - E(0^-) \times d_1 \qquad (2.4.1.5)$$

Eq. (2.4.1.3) together with Eq. (2.4.1.5) can be used to express V_2 as:

$$V_2 = V - \sqrt{\frac{2Jd_2}{\varepsilon_o \varepsilon_r \mu_{p2}}} \times d_1 \qquad (2.4.1.6)$$

Substitution of Eq. (2.4.1.6) in Eq. (2.4.1.1) yields the expression for current density as:

$$J = \frac{9}{8} \frac{\varepsilon_o \varepsilon_r \mu_{p2}}{d_2^3} \left(V - d_1 \times \sqrt{\frac{2Jd_2}{\varepsilon_o \varepsilon_r \mu_{p2}}} \right)^2 \qquad (2.4.1.7)$$

Rearrangement of the above expression gives:

$$V = \sqrt{\frac{8}{9} \frac{Jd_2^3}{\varepsilon_o \varepsilon_r \mu_{p2}}} + \sqrt{\frac{2Jd_1^2 d_2}{\varepsilon_o \varepsilon_r \mu_{p2}}}$$

This is approximately equal to:

$$V \approx \sqrt{\frac{Jd_2}{\varepsilon_o \varepsilon_r \mu_{p2}}} (d_2 + \sqrt{2} d_1) \qquad (2.4.1.8)$$

Thus from the above relation, current density can be expressed in the terms of applied voltage as:

$$J = \frac{\varepsilon_o \varepsilon_r \mu_{p2} V^2}{(d_2\sqrt{d_2} + d_1\sqrt{2d_2})^2} \qquad (2.4.1.9)$$

Inclusion of built-in voltage yields the final expression of current density as:

$$J = \frac{\varepsilon_o \varepsilon_r \mu_{p2} (V - V_{bi})^2}{(d_2\sqrt{d_2} + d_1\sqrt{2d_2})^2} \qquad (2.4.1.10)$$

Eq. (2.4.1.10) implies that the current is still space charge limited, with mobility equal to the blocking-layer mobility, and the effective thickness equal to $\sim\sqrt{d_2}(d_2 + \sqrt{2}d_1)$. Furthermore, the equation can also help to experimentally determine the value of blocking-layer mobility, from the current density-voltage characteristics, provided that the transport layer mobility is greater than the blocking layer mobility: $\mu_{p1} > \mu_{p2}$, and the device structure is similar to that shown in Fig.2.1, for which the model is derived.

Fig.2.9 shows the calculated and simulated current density-voltage *(J-V)* characteristics of different bilayer single-carrier (hole-only) device structures under reverse biased condition, as a function of different transport and blocking layer mobilities. The curves A, B, C, D are obtained for device structures with different hole mobility values tabulated in Table2.1.In all the cases the blocking layer thickness is equal to the transport layer thickness. Figure shows that the values predicted by Eq. (2.4.1.10) are in good agreement with the results obtained with the help of numerical simulator. The match with the simulated curves becomes better at higher applied bias. These results confirm that the current density scales proportionally with the blocking-layer mobility, when the hole mobility in the transport layer mobility is greater than the hole mobility in the blocking layer i.e. $\mu_{p1} > \mu_{p2}$.

Fig.2.10 shows the simulated and calculated curves for the different values of transport-layer and blocking-layer thicknesses, tabulated in Table 2.2. Decrease in the value of the blocking layer thickness results in larger value of the current density. Figure shows that

though the calculated values are approximately equal to the simulated values in magnitude, but the slope of the two curves are not exactly same. The results show that the calculated curves have greater slope than the simulated curves. It is quiet clear that though this particular model is good for crude analysis, it doesn't precisely describe the characteristics of device. As the complete derivation was made under the assumption of bulk-limited conduction and current was modeled with Eq. (2.4.1.1) initially, it is expected that current doesn't exactly follow the trend predicted by Eq. (2.4.1.1). To further explore the behavior in reverse direction we consider the case when the transport layer mobility is less than the mobility in blocking layer.

Table 2.1

	A	*B*	*C*	*D*	*Thickness (microns)*
μ_{p1} *(cm²/V-sec)*	5.00E-05	5.00E-06	5.00E-07	5.00E-07	$d1$=5.00E-02
μ_{p2} *(cm²/V-sec)*	5.00E-07	5.00E-07	5.00E-08	5.00E-09	$d2$=5.00E-02

Table 2.2

	A	*B*	*C*	*Mobility (cm²/V-sec)*
d_1 *(microns)*	0.08	0.02	0.05	μ_{p1}=5.00E-07
d_2 *(microns)*	0.02	0.08	0.05	μ_{p2}=5.00E-09

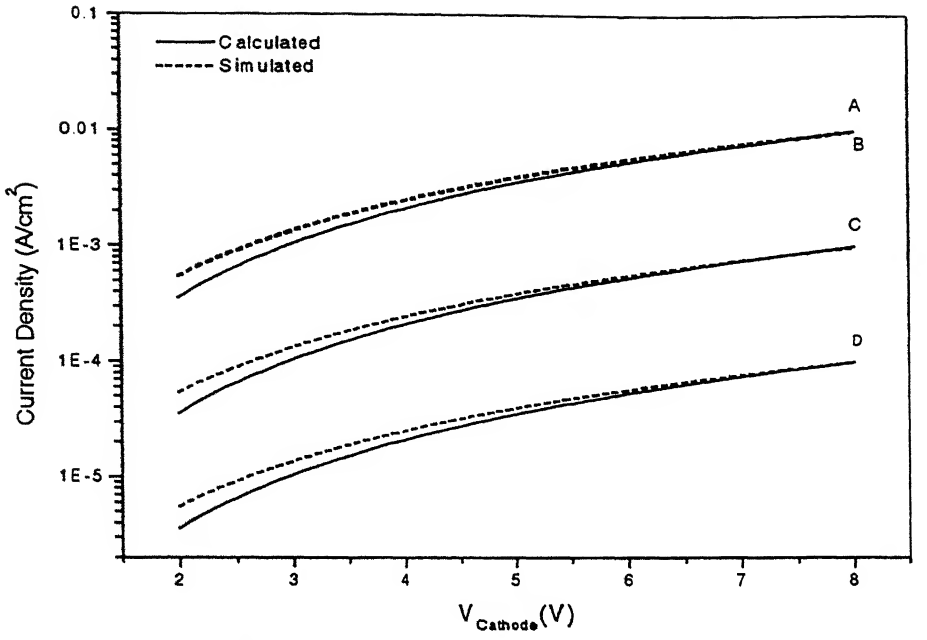

Fig.2.9 Current density as a function of applied bias obtained from the numerical simulation (dotted line) of the device shown in Fig.2.1 and that obtained from Eq.2.4.1.10 (solid line) under reverse bias, for different mobility values mentioned in Table.2.1. The hole (electron) barrier at the organic interface is 0.6eV (0.0eV).

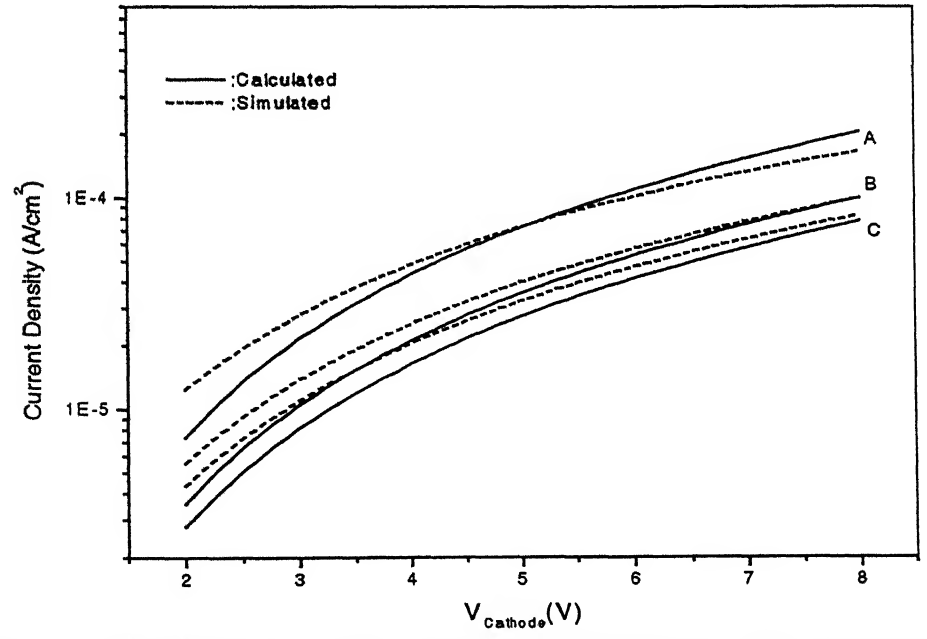

Fig.2.10 Current density as a function of applied bias obtained from numerical simulations (dotted line) of the device shown in Fig.2.1 and that obtained from Eq.2.4.1.10 (solid line) under reverse bias, for different HTL and HBL thicknesses mentioned in Table.2.2. The hole (electron) barrier at the organic interface is 0.6eV (0.0eV).

2.4.2 Case (ii) $\mu_{p1} < \mu_{p2}$.

The simulation results in Fig.2.8 show that the spatial variation of electric field in both the blocking layer and the transport layer is similar to the case of single layer single carrier (hole-only) device. The rate of change of the electric field is characteristic of the hole mobility of the organic material. Under the assumption that the current in the LED compartments is space charge limited rather than injection limited, we have current density in the hole transport layer expressed as:

$$J = \frac{9}{8}\varepsilon_o \varepsilon_r \mu_{p1} \frac{V_1^2}{d_1^3} \qquad (2.4.2.1)$$

To obtain current density in terms of the applied bias V, we need to relate the applied voltage V with the voltage drop across the transport layer V_1. From the fact that the electric field varies as in case of a single layer single carrier device in both the organic layers, we can obtain voltage drop across the blocking-layer by integrating the electric field in the blocking layer [16]:

$$V_2 = \int_{d_2}^{0} \sqrt{\frac{2J(d_2 - x)}{\varepsilon_o \varepsilon_r \mu_{p2}}} dx = \frac{2}{3}\sqrt{\frac{2J}{\mu_{p2}\varepsilon_o \varepsilon_r}} \times d_2^{3/2} \qquad (2.4.2.2)$$

With the help of above expression voltage drop across transport layer (HTL) can be related to applied voltage as:

$$V_1 = V - \frac{2}{3}\sqrt{\frac{2J}{\mu_{p2}\varepsilon_o \varepsilon_r}} \times d_2^{3/2} \qquad (2.4.2.3)$$

Eq. (2.4.2.1) along with Eq. (2.4.2.3) yields:

$$\sqrt{\frac{8}{9}\frac{Jd_1^3}{\varepsilon_o \varepsilon_r \mu_{p1}}} = V - \sqrt{\frac{8}{9}\frac{Jd_2^3}{\varepsilon_o \varepsilon_r \mu_{p1}}}$$

Which can be arranged in a more informative way as:

$$V = \frac{2}{3}\sqrt{\frac{2J}{\varepsilon_o \varepsilon_r}}\left[\sqrt{\frac{d_1^3}{\mu_{p1}}} + \sqrt{\frac{d_2^3}{\mu_{p2}}}\right] \qquad (2.4.2.4)$$

From the Eq. (2.4.2.4), current density can be expressed in terms of applied voltage as:

$$J = \frac{9}{8}\varepsilon_o \varepsilon_r \frac{V^2}{\left(\sqrt{\frac{d_1^3}{\mu_{p1}}} + \sqrt{\frac{d_2^3}{\mu_{p2}}}\right)^2} \qquad (2.4.2.5)$$

Eq. (2.4.2.5) defines the current density-voltage characteristics of the organic light emitting diode for the reverse bias, under the aforementioned mobility condition in the two organic layers. Inclusion of the built-in voltage provides better matching with the simulated characteristics:

$$J = \frac{9}{8}\varepsilon_o \varepsilon_r \frac{(V - V_{bi})^2}{\left(\sqrt{\frac{d_1^3}{\mu_{p1}}} + \sqrt{\frac{d_2^3}{\mu_{p2}}}\right)^2} \qquad (2.4.2.6)$$

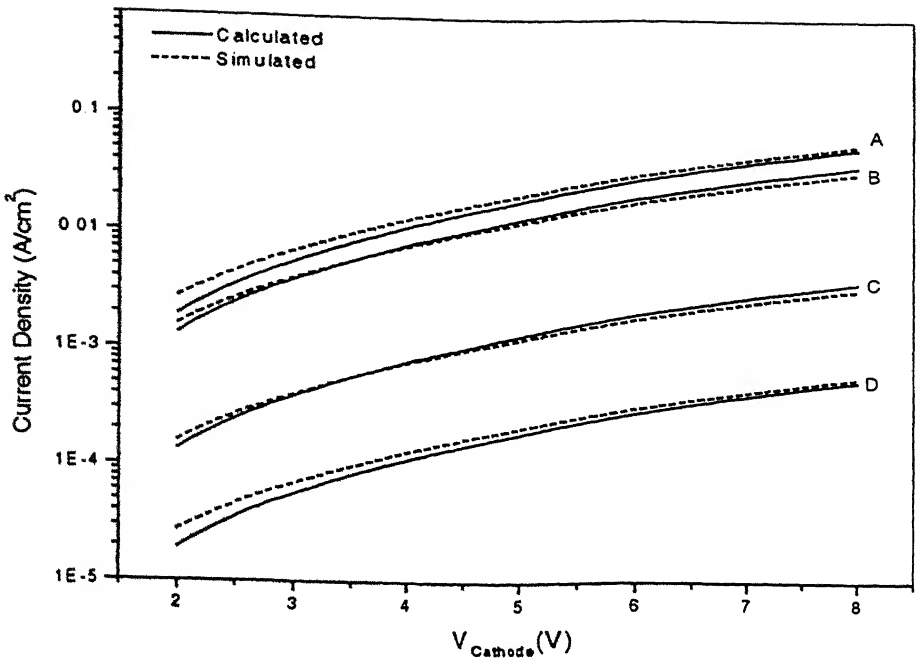

Fig.2.11 Current density as a function of applied bias obtained from numerical simulations (dotted line) of the device shown in Fig.2.1 and that obtained from Eq.2.4.2.6 (solid line) under reverse bias for different mobility values mentioned in Table.2.3. The hole (electron) barrier at the organic interface is 0.6eV (0.0eV).

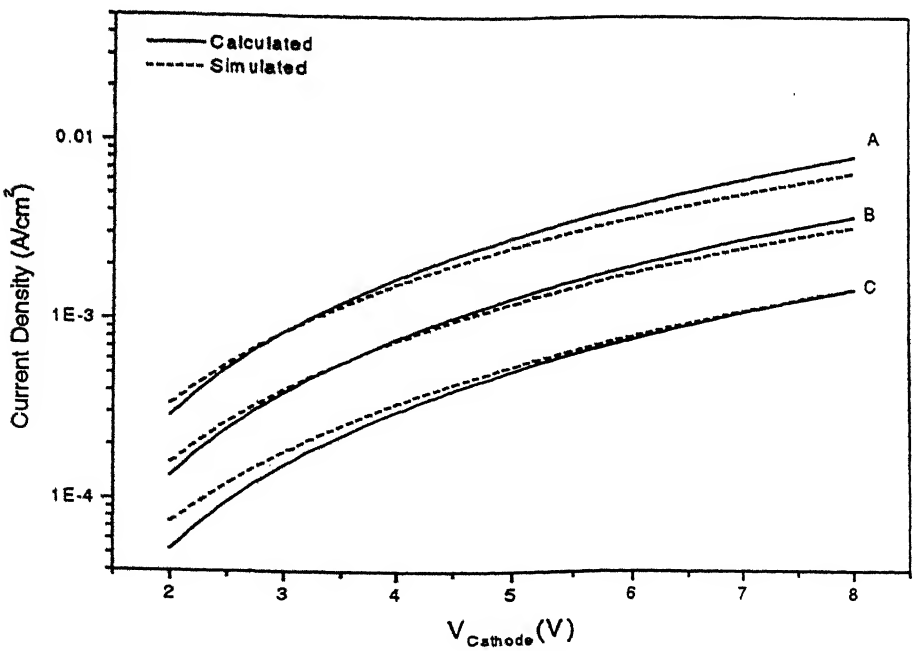

Fig.2.12 Current density as a function of applied bias obtained from numerical simulations (dotted line) of the device shown in Fig.2.1 and that obtained from Eq.2.4.2.6 (solid line) under reverse bias for different HTL and HBL thicknesses mentioned in Table.2.4. The hole (electron) barrier at the organic interface is 0.6eV (0.0eV).

Fig 2.11 shows the simulated and calculated current voltage curves for bilayer device under reverse biased condition, for the different mobility values tabulated in Table2.3. The simulated and calculated values are in good agreement with each other. The simulations were carried out for different values of hole mobility in HTL and HBL, but in each case the transport layer mobility was less than the blocking layer mobility. Fig 2.12 shows current voltage characteristics plotted for different thicknesses of the blocking layer and the transport layer tabulated in Table 2.4. The model developed shows better match with the simulated results, than in the case when $\mu_{p1} > \mu_{p2}$. At the higher applied bias difference between the simulated and predicted value decreases.

Table 2.3

	A	*B*	*C*	*D*	*Thickness (microns)*
μ_{p1} *(cm²/V-sec)*	5.00E-07	5.00E-07	5.00E-08	5.00E-09	$d1$=5.00E-02
μ_{p2} *(cm²/V-sec)*	5.00E-06	5.00E-05	5.00E-07	5.00E-07	$d2$=5.00E-02

Table 2.4

	A	*B*	*C*	*Mobility (cm²/V-sec)*
d_1 *(microns)*	0.02	0.05	0.08	μ_{p1}=5.00E-08
d_2 *(microns)*	0.08	0.05	0.02	μ_{p2}=5.00E-07

Case 2.4.3: $\mu_{p1} = \mu_{p2}$

Up till now we have considered two cases where there was difference in mobility in the blocking layer and the transport layer. The simulations carried out for the device having equal blocking layer and transport layer mobility show, that the field and the charge

profile in such device structures is essentially equal to that of single layer single carrier (hole-only) device which can simply be expressed by space charge limited conduction:

$$J = \frac{9}{8}\varepsilon_o \varepsilon_r \mu_p \frac{V^2}{d^3} \qquad (2.4.3.1)$$

When modeled in terms of space charge limited current, the simulations carried out show good agreement with the values predicted given by Eq (2.4.3.1). Fig 2.14 shows that variation in relative thickness of the hole transport layer and the hole blocking layer has negligible effect on the current density-voltage characteristics in case of the equal mobility of two layers.

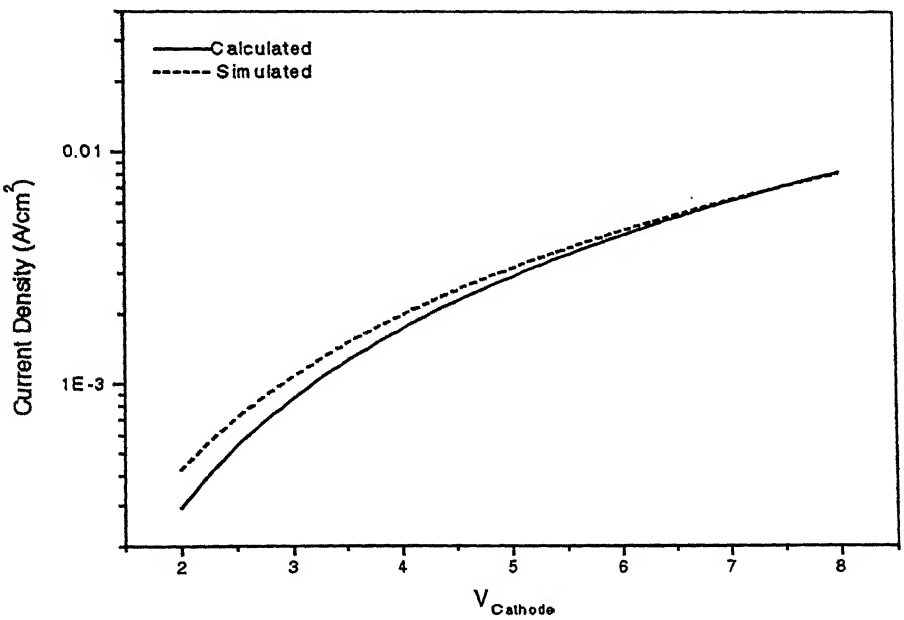

Fig.2.13 Current density as a function of applied bias obtained from numerical simulations (dotted line) of the device shown in Fig.2.1 and that obtained from Eq.2.4.3.1 (solid line) under reverse bias for same hole mobility value of 0.5×10^{-6}cm^2/V-sec in both the layers. The hole (electron) barrier at the organic interface is 0.6eV (0.0eV).

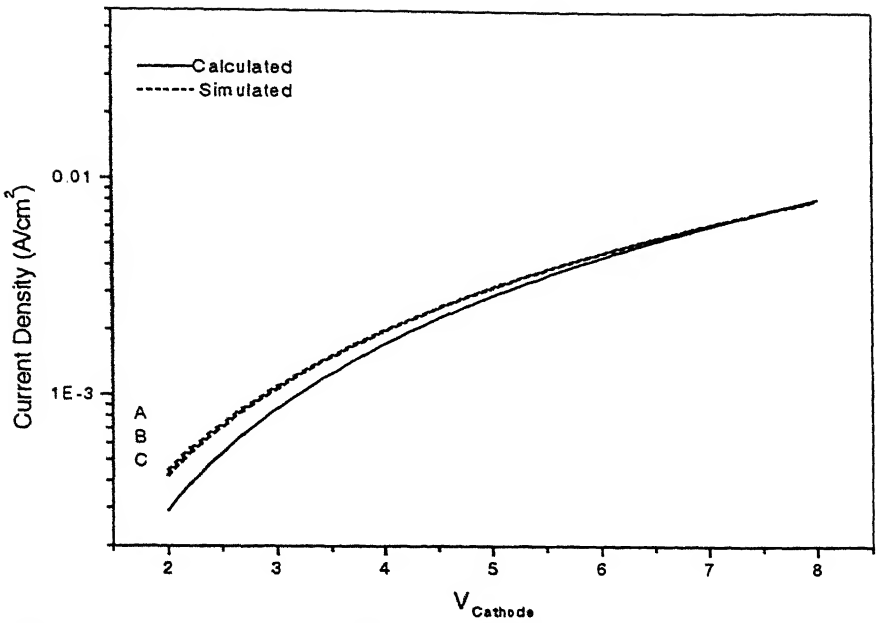

Fig.2.14 Current density as a function of applied bias obtained from numerical simulations (dotted line) of the device shown in Fig.2.1 and that obtained from Eq.2.4.3.1 (solid line) under reverse bias for different HTL and HBL thicknesses mentioned in Table.2.3. The hole (electron) barrier at the organic interface is 0.6eV (0.0eV). Both the layers have an hole mobility of $0.5\times10^{-6}cm^2/V\text{-}sec$.

To summarize, analytical models for the hole-only bilayer organic OLED has been developed. The models developed predict the dependence of current density on the voltage, material thickness and the interface barrier heights in forward direction as well as reverse direction.

Chapter 3

Bilayer device with bipolar injection:

3.1 Introduction: The previous chapter discusses bilayer single carrier structures in which energy barrier to injection of one carrier type is significantly larger than the other, so that the current flow in the device is dominated by single carrier type. Although such structures provide a comparatively simple situation in which to study the operating principles of organic diode, such single carrier structures do not function as LEDs. Devices in which both carrier types are efficiently injected exhibit strong electro-luminescence and meet specifications of target applications.

The properties and mechanisms of physical processes involved in bilayer bipolar devices are subject to analytical as well as numerical investigation. We focus on the study of bilayer devices under bipolar injection condition by developing a simple analytical model that adequately describes the current density-voltage characteristics of the device. In addition to the current voltage characteristics, understanding of operation of an organic LED also requires knowledge of the recombination process involved. In this chapter, a conceptional framework is laid down to qualitatively describe the phenomenon related to charge recombination in organic LEDs. The results interpreted from simulated spatial variation of electric field, charge density and recombination rate density, shows shift in magnitude and peak of the recombination zone, with band offset at organic interface and provide important guidelines for optimizing bilayer LEDs.

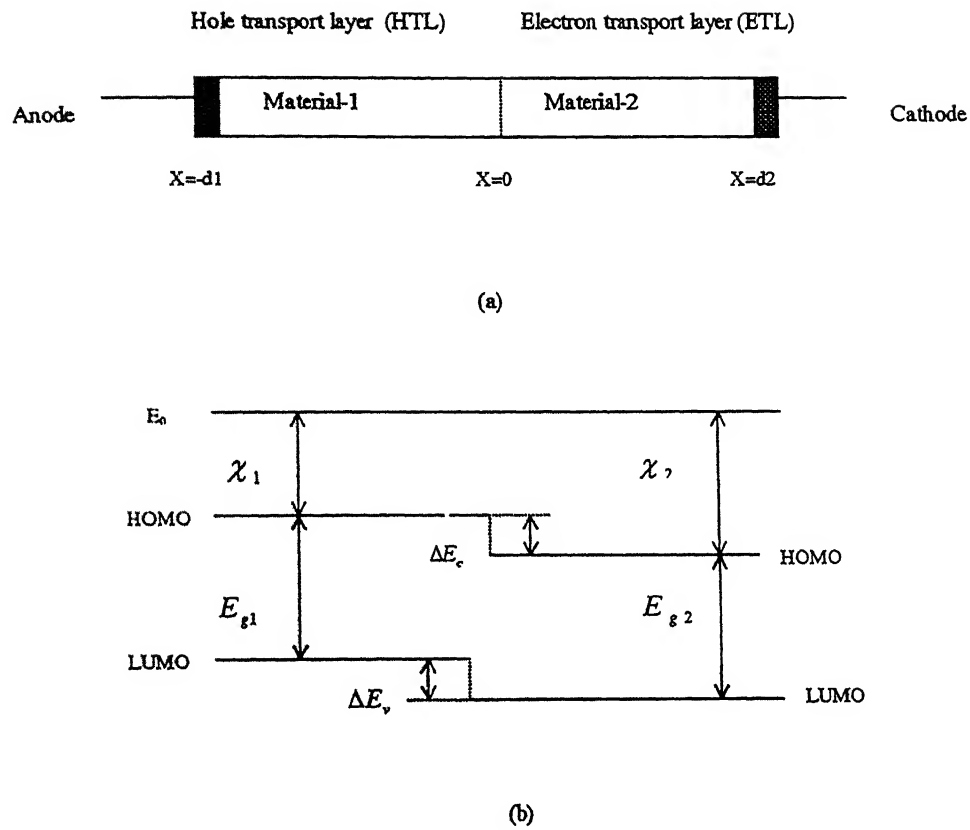

Fig.3.1 (a) Schematic diagram of a bilayer organic LED (b) and its associated energy band diagram.

3.2Analytical Model: To illustrate the performance of a bilayer device under bipolar injection condition, we consider a device structure as shown in Fig.3.1 (a). The device consists of a hole transport layer (material-1) and an electron transport layer (material-2). The associated band diagram under flat band condition is shown in Fig 3.1(b). For simplicity, we assume that there is only a 'valence-band' discontinuity at the organic interface, such that the passage of holes across the internal interface towards the cathode is impeded by an energy barrier of height ΔE_v. We assume that the hole (electron) barrier at anode (cathode) is small enough to provide space charge limited current. The hole

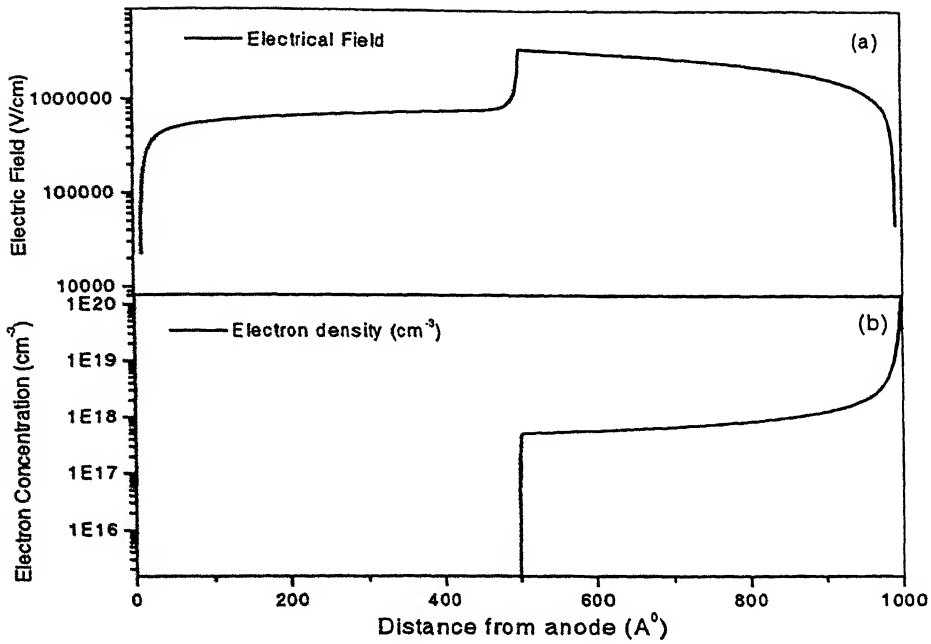

Fig 3.2(a). Electrical field as a function of distance, obtained from the numerical simulation of a bilayer bipolar device. Fig 3.2(b). Electron density as a function of distance obtained from the numerical simulation. The hole barrier ΔE_v is 0.6eV, and electron barrier ΔE_c is 0.0eV at the organic interface. The hole (electron) barrier at the anode (cathode) is 0.2eV(0.1eV). Both layers are of equal thickness and have equal hole (electron) mobility of 0.5×10^{-6} (0.5×10^{-8}) cm^2/V-sec.

(electron) mobility in the electron transport layer is same as the hole (electron) mobility in hole transport layer. But in both the layers, the electron mobility is two orders of magnitude smaller than the hole mobility. The analytical model assumes drift diffusion transport in bulk and thermionic emission at organic interface. Transport of the holes and electrons in both the materials is assumed to be trap free.

Fig.3.2 (b) shows the electron density profile for a bilayer device structure under bipolar injection condition, obtained with the help of numerical simulator. The large hole barrier at the organic interface results in accumulation of holes at the organic interface in HTL, and very low hole density in the right layer (ETL). For the small barrier to electron injection at cathode, large electron density determines the device current in the ETL:

$$J \sim J_n \text{ and } J_p \sim 0 \text{ for } x \geq 0 \qquad (3.2.1)$$

The simulation results suggest that the electric field and electron density profile in the electron transport layer is similar to that of a single layer electron only device. This behavior is very well theoretically justified because of the presence of small electron energy barrier at the cathode and large hole energy barrier at the organic interface. Then under bulk-limited trap free condition, current in ETL can be described by SCLC as:

$$J = \left(\frac{9}{8}\right)\mu_{n2}(\varepsilon_0\varepsilon_r)\frac{V_{ETL}^{\ 2}}{d_2^{\ 3}} \qquad (3.2.2)$$

where V_{ETL} is the voltage drop across electron transport layer. The bilayer device structure has a much higher electric field in the right layer. This higher value of the electric field is required to drive electron current with low electron mobility. Thus, it can be assumed without much error that all the applied voltage is used to drive low mobility electrons in the electron transport layer:

$$V \approx V_{th} \qquad (3.2.3)$$

Eq. (3.2.2) along with the Eq. (3.2.3), can now be used to express the current density in terms of applied voltage as:

$$J = \left(\frac{9}{8}\right)\mu_{n2}(\varepsilon_0\varepsilon_r)\frac{V^2}{d_2^{\ 3}} \qquad (3.2.4)$$

Eq. (3.2.4) suggests that the bilayer device under bipolar injection condition, behaves as a single layer electron only device, with effective length equal to the electron transport layer thickness d_2, and mobility equal to the electron mobility μ_{n2} in ETL.

However in case of bipolar devices, there is significant difference between the work function of anode and cathode, and a built in potential V_{bi}, is established in the organic layer at zero bias. This built in potential fundamentally affects the operating characteristics of diode. In the simple picture, V_{bi} is equal to work function difference between anode and cathode ($V_{bi} = \phi_h - \phi_e$). To properly characterize the device, this built-in potential must be subtracted from the applied bias:

$$J = \left(\frac{9}{8}\right)\mu_{n2}(\varepsilon_0\varepsilon_r)\frac{(V - V_{bi})^2}{d_2^{\,3}} \qquad (3.2.5)$$

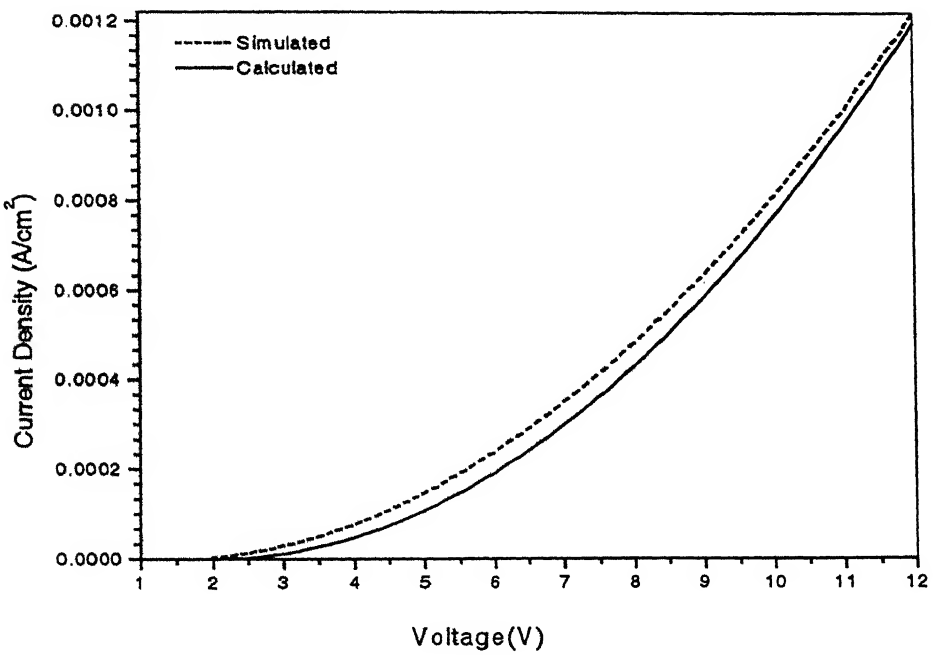

Fig 3.3: Current density of a bilayer device under bipolar injection condition, as a function of applied bias obtained by numerical simulation (dotted line) and that obtained from Eq. (3.2.5) (solid line). The hole energy barrier at the organic interface is 0.6eVand electron energy barrier at the interface is 0.0eV. The hole (electron) mobility in ETL and HTL is 0.5×10^{-6} (0.5×10^{-8}) cm^{-2}/V-sec.

Fig. 3.3 shows that the current density predicted by the above expression, matches very well with the simulated results at higher voltages. The onset of *J-V* curves is shown from 2V in the figure. It was observed during simulations that at low voltage values match is

not as good as at high voltage values. This is because at low voltages built-in voltage affects the operating characteristics of diode. For an applied bias less than V_{bi}, the electric field inside the diode opposes charge injection and forward drift current, and the current may flow by diffusion [13].

The simulation results shown in figure were carried out for a device structure having hole barrier of 0.6eV at the organic interface. However Eq. (3.2.5) has been obtained without any reference to the magnitude of 'valence-band' discontinuity ΔE_v at the organic interface. This implies, that the equation should hold good irrespective of any value of ΔE_v, provided ΔE_v is large enough to efficiently block the passage of holes towards the cathode.

Fig 3.4 shows comparison of current density–voltage characteristics obtained with the help of numerical simulator and those obtained from Eq. (3.2.5) as a function of different ETL thicknesses. Comparison between the simulated and calculated curves show that for smaller value of the ETL thickness proposed model overestimates the current. This is because, while developing the analytical model it was assumed that nearly all the applied voltage is used to drive electron current with low mobility electrons. As the thickness of ETL decreases lesser fraction of the applied voltage will be used to drive electron current in the ETL. For larger thickness of the ETL, there is better matching between the simulated and calculated curves. However contrary to the expectation, the simulated value of the current overestimates the calculated value of the current. The reason for this behavior in the calculated and simulated current values couldn't be properly justified from the steps involved and assumptions made to derive the model, and is a question of further study.

It can be observed from the Eq. (3.2.5) that the current density is dependent on the electron mobility μ_{n2}, in electron transport layer. Fig.3.5 shows that the model correctly describes the dependence of current density on the electron mobility in ETL. While doing numerical simulations, ratio of hole and electron mobility in ETL and HTL is kept

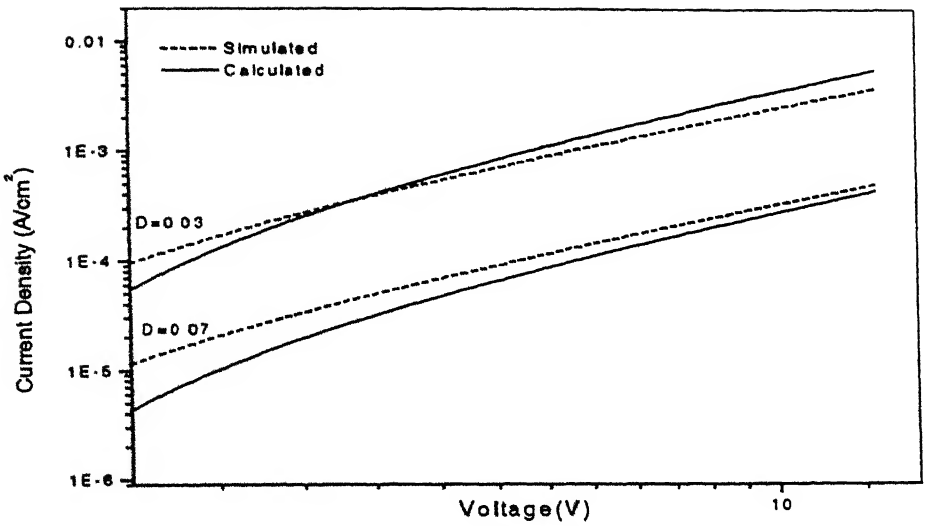

Fig 3.4:Current density-voltage characteristics obtained from numerical simulation (dotted-line) and that obtained from Eq. (3.2.5) (solid line) as a function of different electron transport layer (ETL) thicknesses for a bipolar bilayer device. Characteristics are obtained for the hole barrier ΔE_v of 0.6eV and the electron barrier ΔE_c of 0.0eV at the organic interface. The hole (electron) barrier at anode(cathode) is 0.2eV(0.1eV), and the hole (electron) mobility is 0.5×10^{-6} (0.5×10^{-8}) cm^2/V-sec in both the layers.

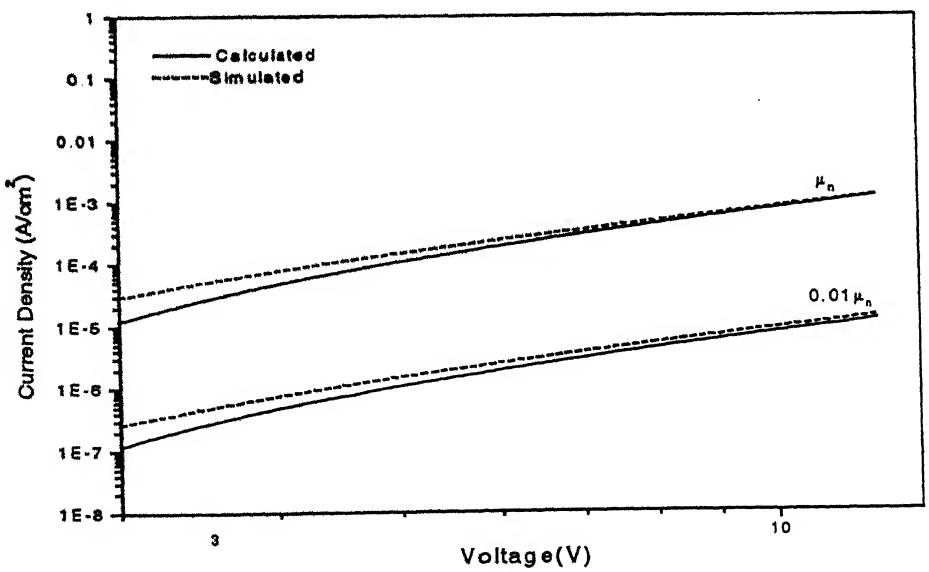

Fig 3.5:Current density-voltage characteristics obtained from numerical simulation (dotted line) and that obtained from Eq. (3.2.5) (solid line) as a function of different electron mobility in ETL for a bilayer bipolar device. Characteristics are obtained for the hole barrier ΔE_v of 0.6eV and the electron barrier ΔE_c of 0.0eV at the organic interface. The hole (electron) barrier at anode (cathode) is 0.2eV(0.1eV), and the hole (electron) mobility is 0.5×10^{-6} (0.5×10^{-8}) cm^2/V-sec in both the layers.

constant, such that the assumption of all the applied voltage driving the low mobility electrons is justified. Figure shows that the current density scales with the mobility of electron in the electron transport layer. However the simulated value of the current density exceeds the calculated value. The reason for this behavior couldn't be properly explained from the assumptions made while arriving at the analytical model.

Furthermore, the analytical model was derived without any reference to recombination process. This is because, in view of bimolecular nature of the recombination, there are very few holes available on the other side of the hole barrier in ETL to recombine with the incoming electron flux. Thus we assume that the error caused in making this assumption is very less. However an understanding of fundamentals of the LED operation also requires detailed knowledge of the recombination process involved. In the next section we address the problem of recombination that is too important to be ignored

3.3 Recombination: Electro-luminescence from organic LED is the result of formation of emissive excited state via recombination of pair of charge carriers injected from the electrodes. For efficient recombination it is necessary that the local space charge density is very high. This is certainly enhanced in heterojunction devices where confinement at the heterojunction causes buildup in space charge. We investigate the effect of the 'valence-band' and 'conduction–band' offset at the organic interface on the profile and magnitude of space charge buildup, and hence on the radiative recombination.

We consider a bilayer device structure as shown in Fig 3.1(a). We assume that there is 'valence-band' as well as 'conduction–band' discontinuity at the organic interface. We also assume that the hole (electron) injection barrier at the anode (cathode) is small enough 0.2eV(0.1eV), so that maximum carriers are confined in the LED compartment resulting in maximum recombination. The hole and electron mobility in material-1 and material-2 are same. To study the effect caused by the 'valence-band' and 'conduction–band' offset, on the peak and position of recombination zone, we keep the 'valence-band' discontinuity ΔE_v equal to 0.6eV, and change the 'conduction-band' discontinuity ΔE_c from 0.0-1.0eV by varying the bandgap and ionization potential of material-2. Fig 3.6

shows recombination profile in the vicinity of organic interface. Recombination value to the left of organic interface in the hole transport layer is denoted by $U(0^-)$, and that to the right of organic interface in ETL is denoted by $U(0^+)$.

Fig 3.6 shows, that for smaller values of 'conduction–band' discontinuity, maximum recombination occurs to the left of organic interface and recombination in the electron transport layer is very low. But, as ΔE_c is increased maximum recombination peak shifts to the right of interface and magnitude of recombination peak to the left of interface successively decreases. This transition in the shift of maximum recombination peak from HTL to ETL is quiet sharp. For ΔE_c greater than or equal to 0.6eV maximum recombination peak is centered in the ETL. To understand the trend followed in the shift of maximum recombination peak and position, it is useful to consider the electric field,

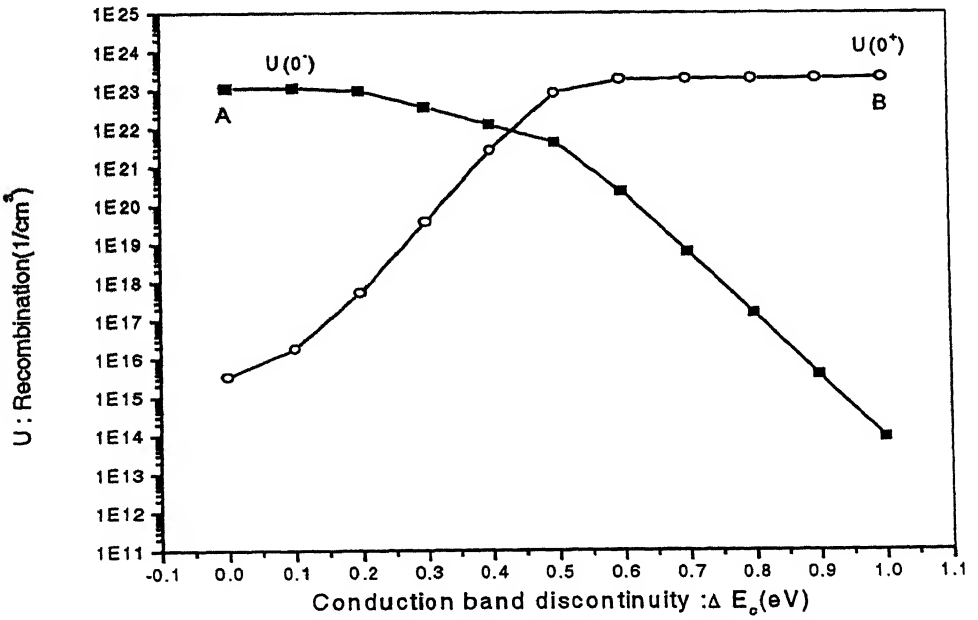

Fig 3.6 Recombination density in the vicinity of the organic interface for different values of electron barrier height at the organic interface for a bilayer bipolar device. The valence band offset is kept equal to 0.6eV. U(0⁻) denotes recombination peak to the left of interface, and U(0+) denotes recombination peak to the right of interface. The hole (electron) barrier at anode (cathode) is 0.2eV(0.1eV) in both the layers.

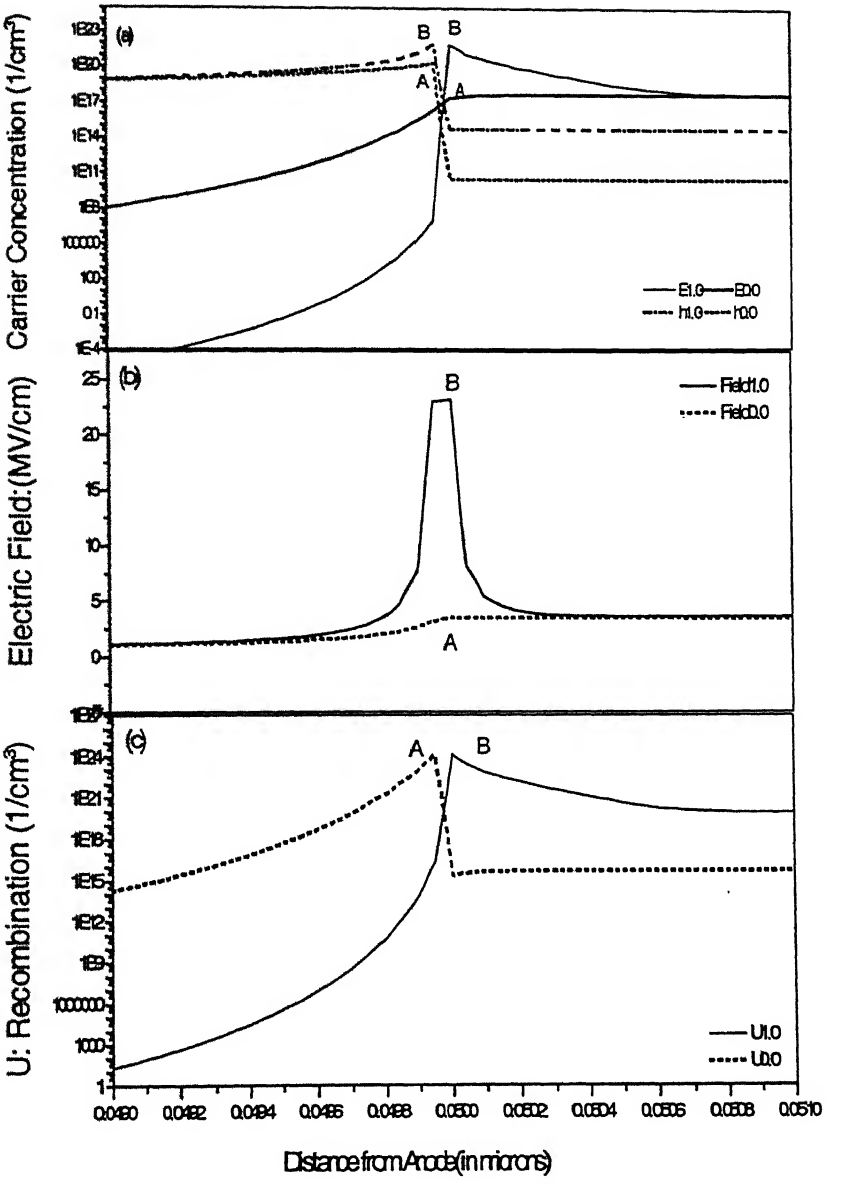

Fig 3.7 (a) Shows variation of electron and hole density, **Fig 3.7** (b) Shows variation of electric field, **Fig 3.7** (c) Shows variation of recombination rate profile, corresponding to point A and B mentioned in Fig 3.6. Point A corresponds to hole barrier ΔE_v of 0.6eV, and electron barrier ΔE_c of 0.0eV at the organic interface. And the point B corresponds to the hole barrier ΔE_v of 0.6eV, and electron barrier ΔE_c of 1.0eV at the organic interface. The hole (electron) barrier at anode (cathode) is 0.2eV(0.1eV), and hole (electron) mobility is 0.5×10^{-6} (0.5×10^{-8}) cm^2/V-sec.

carrier density and recombination rate profile as well. Fig 3.7 shows sectioned view of electric field, carrier density and recombination near the organic interface. To provide an elaborate qualitative explanation that is able to account for the nature of maximum recombination peak shift with the conduction band offset, we take two diametrically opposite points A and B on the curve as shown in Fig.3.6.

Corresponding to point A, the holes traversing from anode towards cathode face a barrier of 0.6eV at the organic interface, but electron flux traversing from cathode towards anode does not face any barrier. The presence of barrier for holes results in large accumulation of holes to the left side of interface but few holes to the other side of interface. The accumulated holes to the left of organic interface, encounters incoming electron flux, resulting in high recombination peak $U(0^-)$ to the left of organic interface. The fact that there are large electrons but few holes available to recombine to the right of interface results in the small value of recombination peak $U(0^+)$.

At point B, ΔE_c is equal to 1.0eV and ΔE_v is equal to 0.6eV at organic interface. This results in a large hole concentration to the left of interface and large electron concentration to the right of interface. The presence of high charge density on the two sides of interface increases the electric field at the interface. The increased field further results in the high accumulation of holes to the left of organic interface, such that hole density to the left of interface is nearly equal to the electron density to the right of organic interface. The magnitude of the recombination peak to the left side of interface is a function of number of electrons that can cross the electron barrier from ETL towards HTL. Similarly recombination peak to the right side of interface is a function of holes that can cross the hole barrier at the interface, and move from HTL towards ETL. Despite the presence of equal electron and hole concentration on the two sides of the barrier, fact that there exists lower hole barrier at the organic interface results in increase in the fraction of holes making it to the other side of interface and thereby high $U(0^+)$. The small number of electrons crossing the barrier towards HTL results in the smaller value of recombination peak to the left side of interface.

The intermittent points between A and B can be explained in view of branching ratio of the carriers remaining to the one side of the interface and those making it to the other side of the interface. Furthermore branching between the recombination and carrier drift results from complex interplay between charge accumulation and field assisted barrier crossing with the change in electron and hole offsets at the interface, which affects the profile of recombination rate in LED.

Fig 3.7 shows that once maximum recombination peak shifts in ETL, recombination zone becomes evenly spread and confined in ETL layer thereby resulting in superior performance as LED. In view of bimolecular nature of recombination an important guiding principal for LED operation is to increase the bipolar charge density stored in the active layer. Fig 3.7 shows that for ΔE_v equal to 0.6eV and conduction band offset greater than or equal 0.6eV, electron and hole densities are more evenly spread through the electron transport layer, with peak carrier densities occurring at heterojunction, resulting in an improved recombination profile in electron transport layer. Thus control of interface may be among more important determining factors in the eventual success of LED.

Following the trend seen in shift of the peak and magnitude of recombination zone with change in conduction-band offset at the organic interface, we further investigate the effect of conduction band discontinuity under similar conditions on current voltage characteristics. Fig 3.8 shows the current voltage characteristics obtained as a function of different values of conduction-band offset. It can be seen that all the curves nearly fall on each other and bunch together. However surprisingly current values for higher 'conduction-band' discontinuity is greater than the cases with no 'conduction-band' discontinuity at the offset. Explanation of this behavior stems from the fact, that presence of high electron barrier increases the accumulation of holes on the other side of junction, which in turn enhances the fraction of holes making it to the other side of barrier.

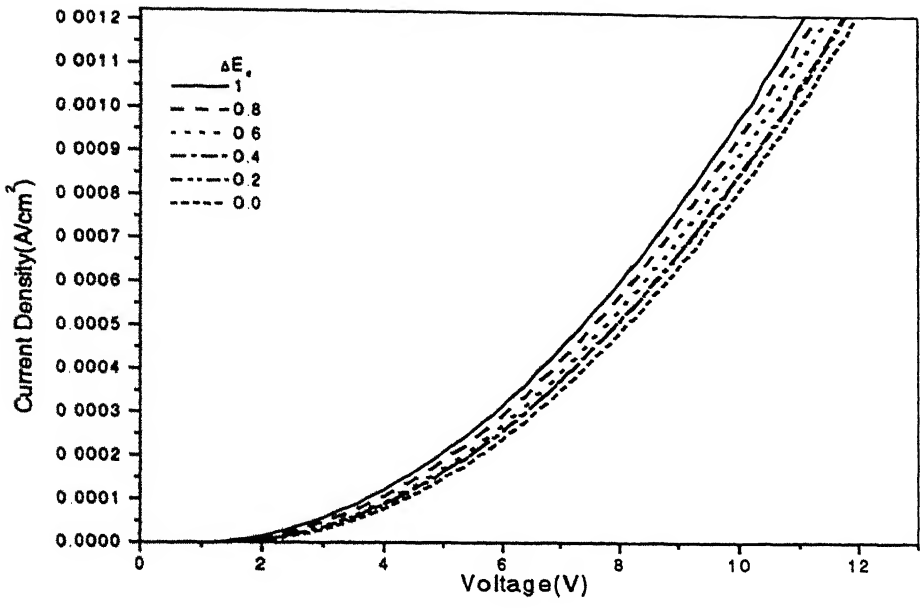

Fig 3.8 Simulated current density-voltage characteristics for the bipolar bilayer devices, as a function of electron energy level discontinuity at the organic interface. The valence level discontinuity is kept equal to 0.6eV in all cases. The hole (electron) barrier at the anode (cathode) is 0.2eV(0.1eV), and hole (electron) the mobility is 0.5×10^{-6} (0.5×10^{-8}) cm^2/V-sec in both the layers.

The presence of high mobility holes in ETL requires smaller voltage to attain the same value of current density. Another important inference that can be drawn from Fig.3.8 is: that the analytical model derived in section 2.2 is valid for structures having conduction-band discontinuity as well.

Almost similar behavior in the recombination profile centered near heterojunction is observed when the 'valence-band' offset is varied from 0.0eV to 1.0eV and the 'conduction-band' discontinuity is kept equal to 0.6eV. Fig. 3.9 shows the recombination rate profile with change in the 'valence-band' discontinuity. Corresponding to point B, hole barrier at the interface is 1.0eV and electron barrier is 0.6eV.The electron and the hole barriers at the interface, results in high hole concentration in HTL and high electron concencentration in ETL. The lesser electron barrier results in more electrons traversing towards hole transport layer and thereby resulting in high recombination peak $U(0^-)$ in HTL. At point

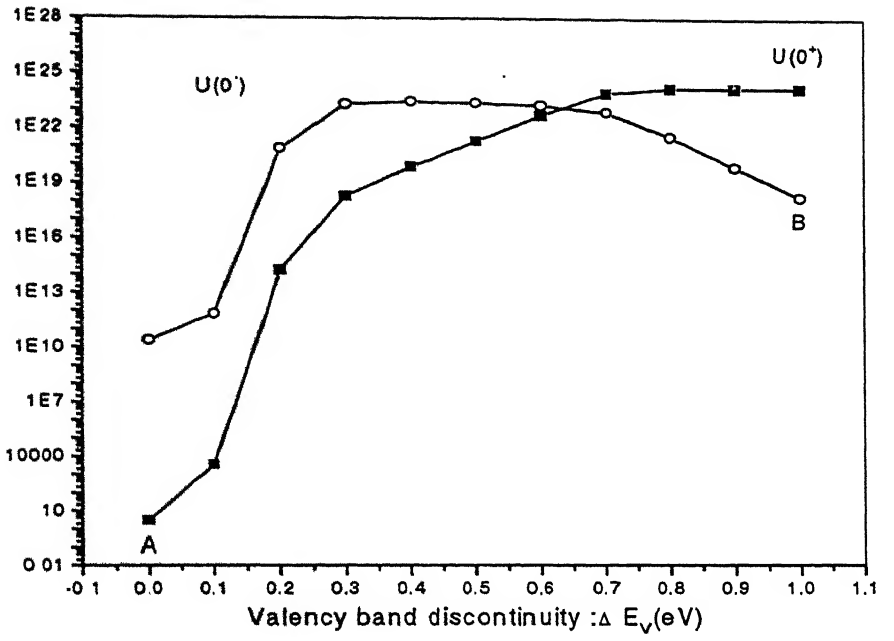

Fig 3.9 Recombination density in the vicinity of the organic interface for different values of hole barrier height at the organic interface for a bilayer bipolar device. Conduction band offset is kept equal to 0.6eV. U (0^-) denotes recombination peak to the left of interface, and U(0^+) denotes recombination peak to the right of interface. The hole (electron) barrier at anode (cathode) is 0.2eV(0.1eV)), and the hole (electron) mobility is 0.5×10^{-6} (0.5×10^{-8}) cm^2/V-sec in both the layers.

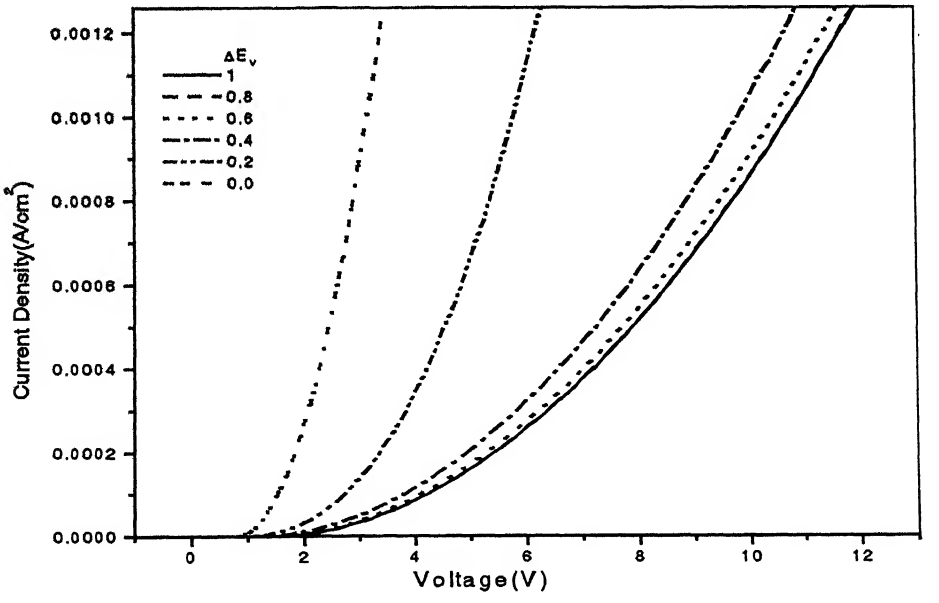

Fig 3.10 Simulated current density-voltage characteristics for the bipolar bilayer devices as a function of hole energy level discontinuity at organic interface. The electron level discontinuity is kept equal to 0.6eV in all cases. The hole (electron) barrier at the anode (cathode) is 0.2eV(0.1eV)), and the hole (electron) mobility is 0.5×10^{-6} (0.5×10^{-8}) cm^2/V-sec in both the layers.

A there is no hole barrier at the interface. The high mobility holes traversing towards cathode prevent the accumulation of electrons at the organic interface. This result is highest recombination peak to be centered near cathode (electron injecting contact). The trend observed in current density-voltage characteristics as a function of hole discontinuity is different from what was observer in Fig.3.8. The difference in the magnitude and behavior of *J-V* curves stems from the fact that for lower hole barrier at the interface, large density of holes cross the barrier and reach the electron transport layer. Smaller value of applied bias will be required to attain the same value of current density because of presence of large hole density in ETL, with hole mobility greater than that of electrons. The current-voltage characteristics are thus more sensitive to hole barrier at the interface due to higher hole mobility.

To summarize the magnitude and position of recombination peak is heavily dependent upon the relative magnitude of electron and hole energy level offsets at interface. A more evenly spread recombination rate can be achieved through the choice of proper offsets at the interface. From Fig.3.6 it can be observed that best device performance regarding recombination rate is achieved for 'valence-band' offset of 0.6eV, and when 'conduction band' offset ΔE_v is kept $\geq 0.6eV$. This results in recombination profile, which is significant throughout the electron transport layer rather then merely at the contacts or heterojunction.

Chapter 4

Criteria for bulk limited conduction

4.1 Introduction:

The current in a bilayer device is denoted by the injection and transport of carriers at the interface. At high injection barriers, the number of charge carriers injected into the bulk per second, is limited by the height of the potential barrier at the contact, and the current regime is thus said to be *contact limited.* Lowering the injection barrier will eventually lead to a situation where the organic material is no longer able to transport injected charge carriers sufficiently fast across the bulk. A space charge will thus arise within the bulk, and the current regime is said to be *space charge limited' or' bulk-limited* [9].

In the models developed so far, it was assumed that the current is bulk limited. In this chapter we develop analytical models that define the range of energy barrier at the contact, when the condition of bulk-limited transport is likely to hold good in the device. Furthermore, since the bilayer device structure enhances the space charge confined in LED compartments, we try to model the effect of band discontinuity in bilayer devices, in maintaining the bulk-limited conduction.

4.2:The Device Physics:

Theoretical modeling of the charge injection has been attempted by several approaches [10-13]. In this section the model for charge injection is outlined. The model assumes injection to be a combination of thermionic emission and quantum mechanical tunneling,

but with the important feature of thermionic backflow. The hole current density flowing across the contact can be expressed as [12]:

$$J_p(0) = J_{th} - J_{ir} + J_{tu} \tag{4.2.1}$$

where J_{th} is the thermionic emission current density, J_{ir} is the back flowing interface recombination current density, and J_{tu} is the tunneling current density. A simple model for the thermionic emission current density is:

$$J_{th} = AT^2 \times \exp(-\phi_h / kT) \tag{4.2.2}$$

where A is Richardson's constant. Because of the image force, the Schottky energy barrier to hole injection ϕ_h depends on the electric field at the interface as:

$$\phi_h = \phi_{ho} - e\sqrt{\frac{eE(0)}{\varepsilon_0 \varepsilon_r}} \tag{4.2.3}$$

The image force barrier lowering term is only included, if the electric field has the correct sign. The interface recombination current density is proportional to the hole density at interface:

$$J_{ir} = vp(0) \tag{4.2.4}$$

The kinetic coefficient v is determined by detailed balancing between thermionic emission and interface recombination. The tunneling current density is calculated using the WKB approximation for tunneling through a potential given by the image force model. Tunneling is only possible if the electric field at the interface has the correct sign:

To determine the kinetic coefficient v it is necessary to specify an equilibrium model for the polymer. For the equilibrium description, the polymer is considered to be

made up of a series of conjugated chain segments. Non–degenerate cases are considered so that the occupation probability of a conjugated chain segment by electrons or holes is much less than unity. Let n_0 be the density of the conjugated chain segments multiplied by the number of ways that a chain segment can be occupied by an electron or hole (i.e. its degeneracy). The equilibrium hole density is:

$$p_e(x) = n_0 \times \exp((E_V - e\phi(x) - \psi)/kT) \tag{4.2.5}$$

where $\phi(x)$ is the position–dependent electrical potential and Ψ is the Fermi energy. At a contact the Fermi energy is determined by the metal. Because the potential is continuous across the interface, the equilibrium hole density is:

$$p_e(0) = n_0 \times \exp(-\phi_h / kT) \tag{4.2.6}$$

where the equilibrium value for the electric field at the contact is used to evaluate ϕ_h. Equating the thermionic emission current density, Eq. (4.2.2), and the interface recombination current density, Eq. (4.2.4), at equilibrium determines the kinetic coefficient ν:

$$\nu = AT^2/n_0 \tag{4.2.7}$$

With this value for ν, the thermionic current density can be written as:

$$J_{th} = \nu n_0 \times \exp(-\phi_h/kT) = \nu \times \overline{p} \tag{4.2.8}$$

where $\overline{p}$ is the quasi-equilibrium hole density at the contact including the barrier lowering due to the electric field, $E(0)$.

The net hole current density at x=0 can be written as:

$$J_p(0) = v[\bar{p} - p(0)] + J_{tu} \qquad (4.2.9)$$

where $v \times p(0)$ is the interface recombination current and $v \times \bar{p}$ is the themionic emission current density. At steady state the total particle current does not depend on position. For a single-carrier (hole-only) device there is only one component to the particle current and therefore that component is independent of position and $J_p(0)$ is equal to the net device current density. Eq. (4.2.9) can be solved for $p(0)$:

$$p(0) = \bar{p} + \frac{J_{tu} - J}{v} \qquad (4.2.10)$$

where J is the net device current density. For polymer diodes the device current density is negligible compared to the sum of the thermionic and tunneling current densities so that J can be dropped in the above equation. There are two limiting regimes: One in which the thermionic emission current density is large compared to the tunneling current density so that $p(0) = \bar{p}$, and other in which the tunneling current density is large compared to the thermionic emission current density so that $p(0) = J_{tu}/v$. *The first limit often occurs in polymer LEDs under their usual operating conditions.*

Fig.4.1 compares *J-V* characteristics of device in which cathode is fixed to be Au (4.3eV) and the anode contact is varied to Pt (5.7eV), Cu (4.6eV). The magnitude of the three components of the injected current, that is the thermionic (dotted line), interface recombination (solid line), and tunneling (dotted line) current components, together with the net device current (dashed line) for the devices with Pt, Cu, and Al contacts is shown in the figure. The first panel shows the case of Pt-injecting contact, where the energy barrier to injection is essentially zero (0.05ev) and the current flow is space charge limited. In this case the magnitude of the thermionic emission and interface recombination currents are very large and they almost exactly cancel each other out. The net device current, which is the difference in magnitude between thermionic emission and

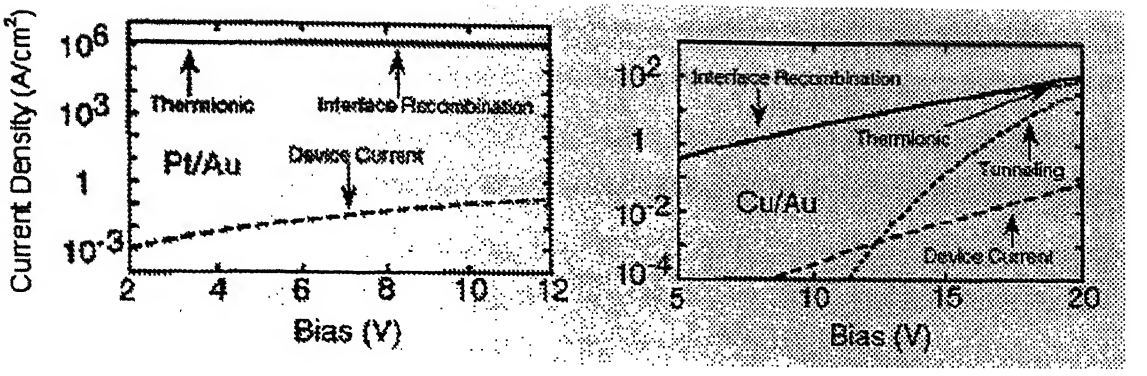

Fig.4.1 Calculated values of injection current components and device current as a function of Bias.

Ref:9 J.Appl. Phys., Vol 82, No 12, 15 December 1997: *' Device model for single carrier organic diodes': P.S.Davis, I.H.Campbell and D.L.Smith*

interface recombination currents, is much smaller than either of these two components separately. There is no tunneling current because the electric field at the contact has the wrong sign for tunneling. The thermionic emission current and interface recombination currents are independent of bias because the applied electric field is completely screened by a large carrier density at the interface and the electric field at the interface has wrong sign for image force barrier lowering.

The second panel of Fig.4.1 shows results for the device with a Cu contact where the energy barrier is increased to 0.6eV and the current flow is contact limited. The magnitude of the thermionic emission and interface recombination components are still much larger than the net device current in this case. The electric field near the contact is no longer screened by a high density of carriers near to the interface, as is the case for the device with a Pt contact and there is image force lowering of the barrier. Therefore, the thermionic emission current is bias dependent and in addition tunneling is possible. Over most of the bias range shown, thermionic emission is much larger than tunneling, but tunneling is a stronger function of the bias than thermionic emission is and at the highest bias shown these two current components become comparable.

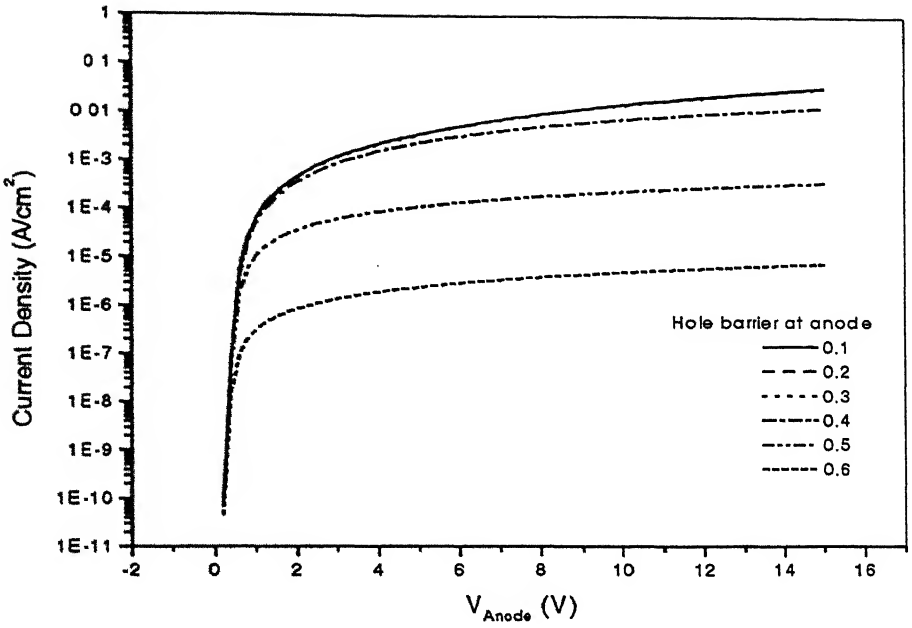

Fig.4.2 (a) Current Density (A/cm^2) plotted with respect to applied bias (V), as a function of different hole barriers at anode, for a single layer hole only device. Electron barrier at the cathode is 1.4eV and the hole (electron) mobility is 0.5×10^{-6}(0.5×10^{-8}) cm^2/V-sec.

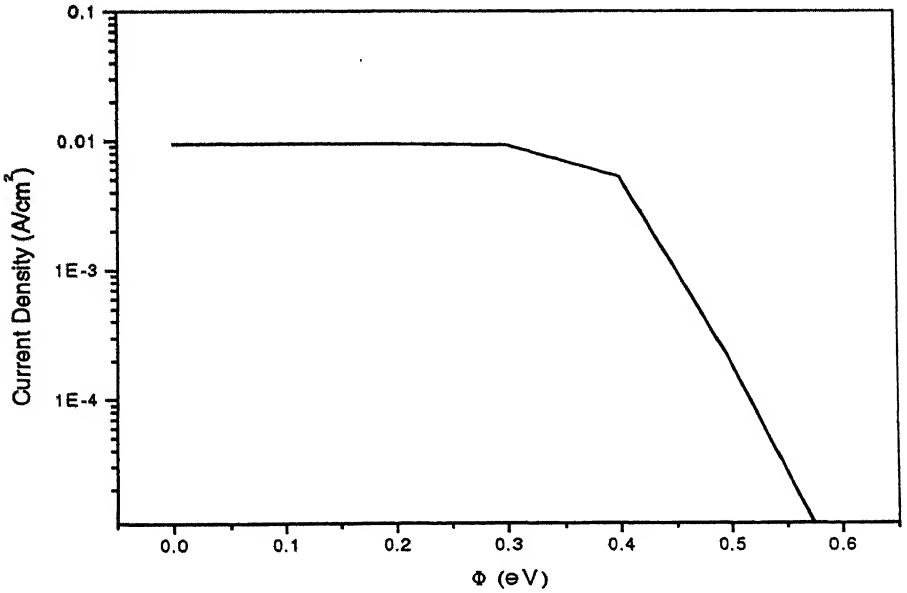

Fig.4.2 (b) Current Density (A/cm^2) plotted with respect to different hole barriers at anode, for a single layer hole only device at an applied bias of 8V. Electron barrier at the cathode is 1.4eV and hole (electron) mobility is 0.5×10^{-6} (0.5×10^{-8}) cm^2/V-sec. The simulation results are obtained at 8V.

Thus for typical polymer LED device parameters current is space charge limited if the energy barrier to injection is less than a particular value and contact limited if it is larger than that. Injection currents have a component due to thermionic emission and a component due to tunneling. For typical polymer LED parameters the thermionic emission current is larger than tunneling current under normal biasing conditions and in all the cases, the net device current is small compared to the largest injection component. Interface recombination almost exactly cancels the injection current; that is, most carriers that are injected into polymer fall back into metal contact. As a result of the very low mobilities of conjugated polymers, only a very small fraction of the injected carriers are extracted from the contact region.

4.3 Numerical simulation and analytical modeling:

Intuitively one expects, that for small energy barrier contacts, space charge effects in the bulk will limit the current flow in a single-carrier device, and for large energy barrier, current flow will be limited by the contacts. To investigate the transition between space charge limited and contact limited current flow, we consider organic diodes, with injection barriers such that holes dominate the current flow. Fig.4.2 (a) shows a log-linear plot of simulated current density-voltage (*J-V*) characteristics and Fig.4.2 (b) shows the variation of current density with respect to hole injection barrier at the anode. The results are obtained by varying anode barrier for hole injection from 0.1eV to 0.6eV in 0.1eV steps. The simulated results for 0.1,0.2 and 0.3eV barriers are nearly the same. For these cases the current is bulk- limited. As the energy barrier is further increased the current is decreased indicating that the current flow becomes contact limited. These results show that, for typical organic LED device, it is important that injection barriers be kept less than value at which transition from bulk-limited to contact limited conduction occurs.

4.3.1Analytical Model: Single layer hole only device structure:

To investigate the transition between bulk limited and contact limited current flow in a single layer device; simulations were carried out for two different device structures. We specifically consider the case in which the energy barrier to injection of electrons is much

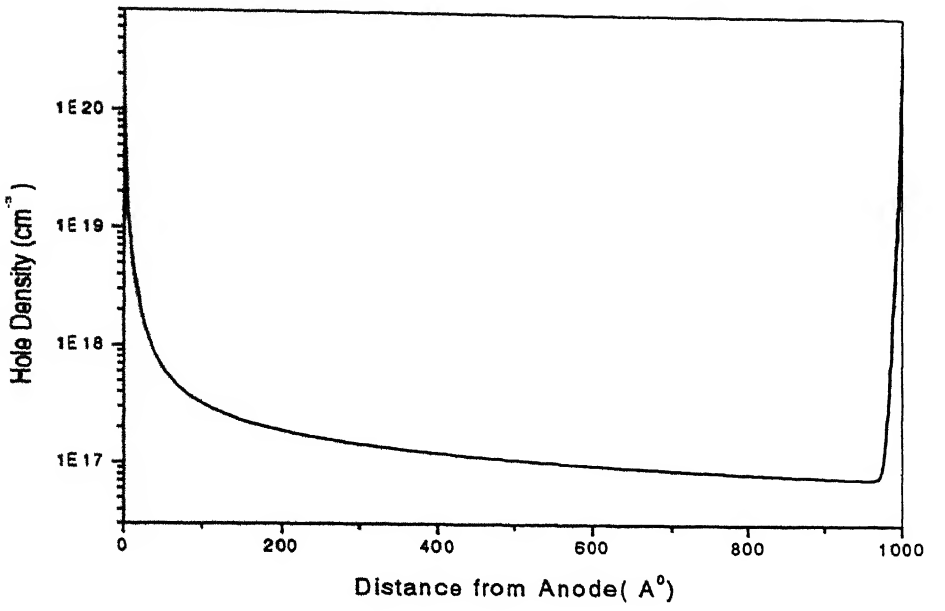

Fig. 4.3a Spatial variation of hole concentration, at an applied bias of 5V, for bulk-limited conduction, for Au/Poly/Au device on Log-Linear scale. The hole (electron) barrier at the anode (cathode) is 0.2eV(2.2eV) and the hole (electron) mobility is 0.5×10^{-6} (0.5×10^{-8}) cm^2/V-sec.

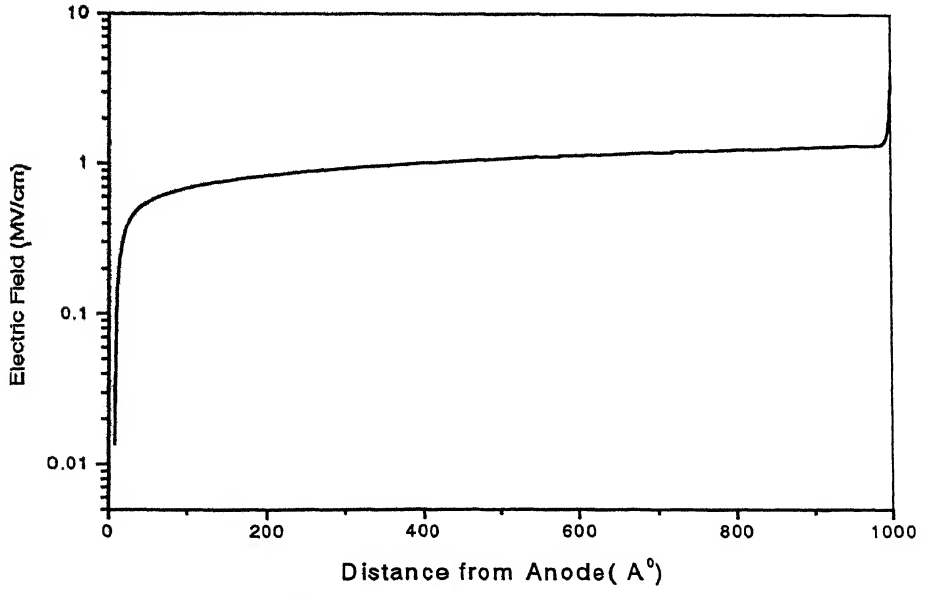

Fig.4.3b Spatial Variation of electric field (MV/cm), for bulk-limited Conduction, at an applied bias of 5V, for Au/Poly/Au device, on Log-Linear scale. The hole (electron) barrier at the anode (cathode) is 0.2eV(2.2eV) and the hole (electron) mobility is 0.5×10^{-6} (0.5×10^{-8}) cm^2/V-sec.

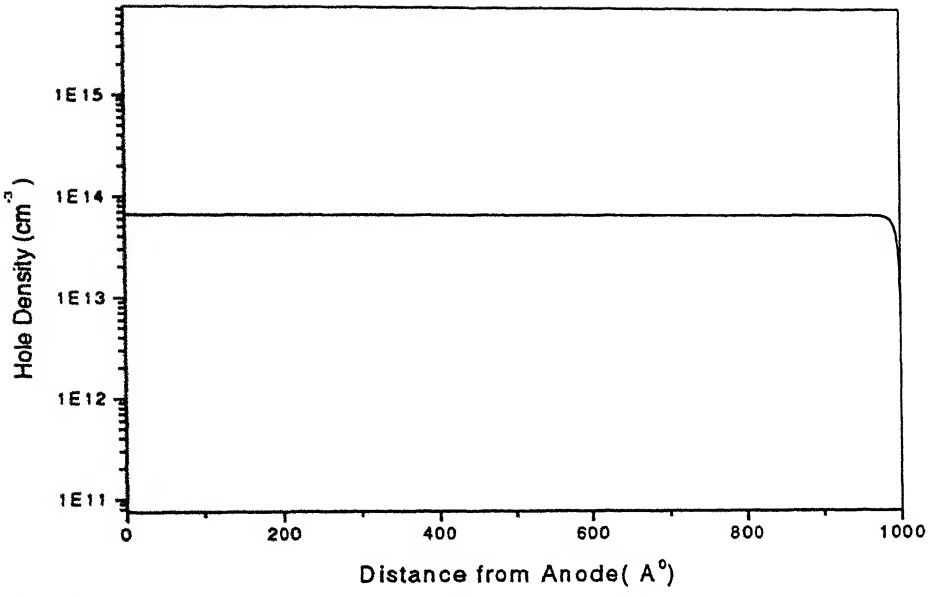

Fig. 4.4a Spatial variation of hole concentration , at an applied bias of 5V, for contact limited conduction, for ITO/Poly/Al device on Log-Linear scale. The hole (electron) barrier at the anode (cathode) is 0.6eV(1.4eV) and the hole (electron) mobility is 0.5×10^{-6} (0.5×10^{-8}) cm^2/V-sec.

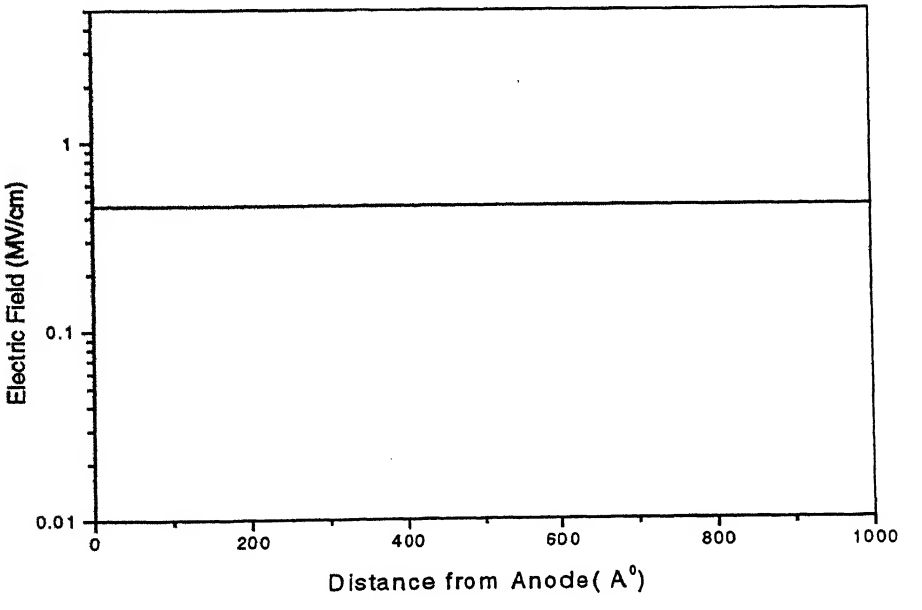

Fig.4.4b Spatial Variation of electric field (MV/cm), for contact limited conduction at an applied bias of 5V, of a ITO/Poly/Al device, on Log-Linear scale. The hole (electron) barrier at the anode (cathode) is 0.6eV(1.4eV) and the hole (electron) mobility is 0.5×10^{-6} (0.5×10^{-8}) cm^2/V-sec.

larger than that for holes, so that the holes dominate the current flow in the device. Fig.4.3a and Fig.4.3b show that for small Schottky energy barriers at anode (0.2eV), the current flow is bulk limited and the electric field in the structure is highly nonuniform. Fig.4.4a and Fig.4.4b show that for larger energy barrier at anode (0.6eV) the current flow is contact limited, the net injected charge is relatively small, the electric field is nearly uniform, and space charge effects are not important.

The simulations carried out suggest that under bulk-limited condition, there is a large accumulation of holes near the hole injecting contact, and hole density decreases with increase in distance from the contact. $(p(0) > p(x) : x > 0)$, however for contact limited current flow, charge density is nearly uniform under the influence of high electric field $(p(0) \approx p(x) : x > 0)$. These results provide foundation for subsequent analytical discussion on the limitations of charge flow across metal-organic interfaces, from which a fairly coherent description of the transition from bulk limited to contact limited regime can be deduced.

Electric field in a single layer hole only device is non-uniform and can be expressed as [16]:

$$E(x) = \sqrt{\frac{2Jx}{\varepsilon_o \varepsilon_r \mu_p}} \qquad (4.3.1.1)$$

Current density for a single layer hole only device, in terms of voltage and interelectrode spacing is given by :

$$J = \frac{9}{8} \varepsilon_0 \varepsilon_r \mu_p \frac{V^2}{d^3} \qquad (4.3.1.2)$$

From the continuity equation, current density can be expressed in terms of electric field and hole density as:

$$J = q\mu_p p(x)E(x) \qquad (4.3.1.3)$$

We neglect the relative magnitude of the diffusion current in terms of drift current, due to poorly characterized diffusion constant and moblities of the polymer. Rearrangement of Eq. (4.3.1.3), and substitution of Eq. (4.3.1.1) in Eq. (4.3.1.3), yields following expressions:

$$qP(x) = \frac{J}{\mu_p}\left(\frac{1}{E(x)}\right)$$

$$qP(x) = \frac{J}{\mu_p}\sqrt{\frac{\varepsilon_r\varepsilon_o\mu_p}{2Jx}}$$

$$qP(x) = \sqrt{\frac{J}{x}} \times \sqrt{\frac{\varepsilon_r\varepsilon_o}{2\mu_p}} \qquad (4.3.1.4)$$

Substitution of Eq. (4.3.1.2) in Eq. (4.3.1.4) gives:

$$qP(x) = \sqrt{\frac{\varepsilon_r\varepsilon_o}{2\mu_p x}} \times \sqrt{\left(\frac{9}{8}\varepsilon_r\varepsilon_o\mu_p\frac{V^2}{d^3}\right)} \qquad (4.3.1.5)$$

This is approximately equal to:

$$qP(x) \approx \frac{\varepsilon_r\varepsilon_o V}{\sqrt{2x}} \times \frac{1}{d^{3/2}} \qquad (4.3.1.6)$$

The hole density at a distance of x=(d/10) from the anode can be obtained from Eq. (4.3.1.6) as:

$$P\left(d/10\right) \approx \frac{1}{q} \times \frac{\varepsilon_r \varepsilon_o V}{d^{3/2}} \times \frac{1}{\sqrt{2 \times (d/10)}} \qquad (4.3.1.7)$$

However from the previous discussions and the simulation results, as long as current is bulk-limited, $\{p(d/10) << p(0)\}$ i.e. hole density at a distance of d/10 away from hole injecting contact, given by Eq. (4.3.1.7), will be less than the hole density injected at the contact:

$$\frac{\sqrt{5}\varepsilon_r \varepsilon_o V}{d^2} << qP(0)$$

'or'

$$qP(0) >> \sqrt{5} \times \left(\frac{\varepsilon_r \varepsilon_o}{d}\right) \times \left(\frac{V}{d}\right) \qquad (4.3.1.8)$$

Eq. (4.3.1.8) states that $p(0)$ is much greater than $p(d/10)$, without any reference to the magnitude by which it exceeds $p(0)$. If a factor ξ is introduced, which takes into account the factor by which hole density at the hole injecting contact exceeds hole density at the distance x=d/10, then Eq. (4.3.1.8) can be expressed as:

$$qP(0)d \geq \xi \times \sqrt{5} V \left(\frac{\varepsilon_r \varepsilon_o}{d}\right) \qquad (4.3.1.9)$$

Above expression can also be better expressed as:

$$Q \geq \xi \times CV\sqrt{5}$$

'or' as:

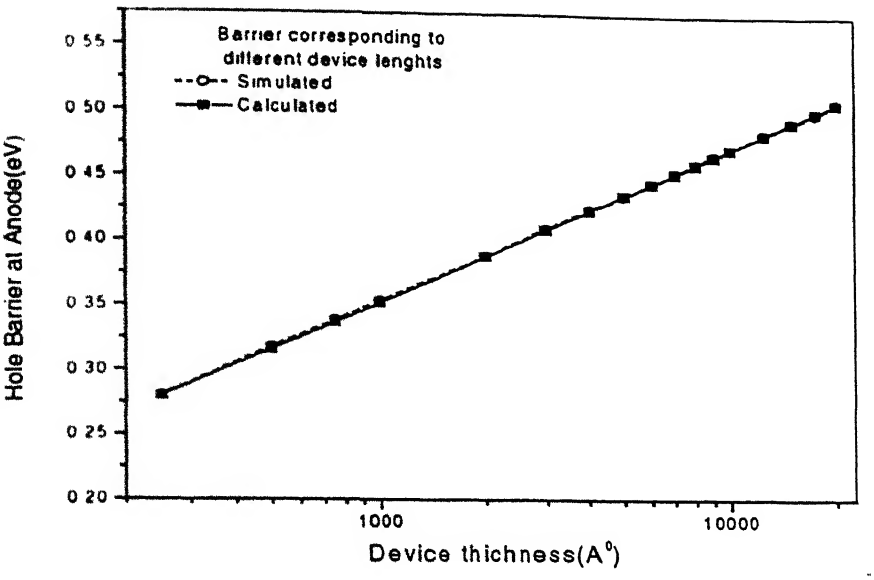

Fig.4.5 Variation in transition point from SCLC to contact limited regime, as a function of different values of device thickness, for a single layer hole only device. Open circle denotes values obtained from simulator and solid square denotes values obtained from Eq. (4.3.1.14) at 5V for ξ=5.6.

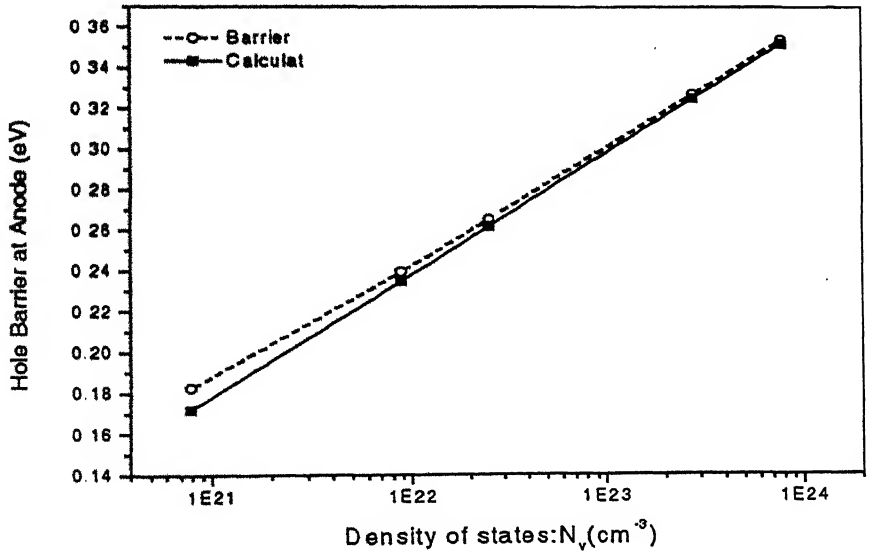

Fig.4.6 Shows variation in transition point from SCLC to contact limited regime as a function of different values of density of states in valence-band for a single layer hole only device. Open circle denotes values obtained from simulator and solid square denotes values obtained from Eq. (4.3.1.14) at 5V for ξ=5.6

ϕ_h will cause the device to operate in the contact limited regime.Fig.4.5 shows barrier height at the anode obtained from the numerical simulator and those calculated by the above expression, for different device thicknesses, ranging from 250 to 20000 Å. The barrier height predicted by the above expression matches exactly with the simulation results on introducing proper value of ξ.

Furthermore, Eq. (4.3.1.14) also shows that the barrier height is also sensitive to the effective density of states in the valence band. Fig.4.6 shows that the barrier height predicted by above expression, for various densities of states N_v, is also in good agreement with the simulated values. For all the calculated values of ϕ_h, value of ξ is adjusted, such that the barrier height predicted by Eq. (4.3.1.14), matches well with the barrier heights obtained by the numerical simulator.

4.3.2.Analytical model: Bilayer hole only device:

From the discussion on the operating principles of device it is clear that thermionic injection is the rate-limiting phenomenon. Thermionic current can be expressed as [15]:

$$J_{th} = qvn_0 \times \exp(-\phi_h / kT) \qquad (4.3.2.1)$$

Where v is the thermal velocity, n_0 is density of conjugated chain segments multiplied by number of ways that electrons or holes can occupy a chain segment. Eq. (4.3.2.1) gives the maximum value of current density that contact is capable of supplying. At zero energy barrier to hole injection, contact can supply maximum current. With increase in energy barrier at contact the amount of carriers, and hence the current injected in the organic layer decreases.

From the expression derived in chapter2, current density in a bilayer hole only device, can be expressed as:

$$J_p = \varepsilon_0 \varepsilon_r \times \mu_p \times \frac{q}{kT} \times (\frac{V - V_{bi}}{d_2})^3 \times \exp(-\Delta E_v / kT) \qquad (4.3.2.2)$$

From the definition of bulk-limited conduction, as long as the current supplied by contact is greater than the current conducting capacity of the bulk, we assume that the device operates in bulk-limited regime. This can be expressed quantitatively from Eq. (4.3.2.1) and Eq. (4.3.2.2) as:

$$\varepsilon_0 \varepsilon_r \times \mu_p \times \frac{q}{kT} \times (\frac{V - V_{bi}}{d_2})^3 \times \exp(-\Delta E_V / kT) << q v n_o \times \exp(-\phi_h / kT)$$

'or' as:

$$\varepsilon_0 \varepsilon_r \times \mu_p \times \frac{q}{kT} \times (\frac{V - V_{bi}}{d_2})^3 \times \exp(-\Delta E_V / kT) \leq \frac{1}{\xi} q v n_o \times \exp(-\phi_h / kT) \qquad (4.3.2.3)$$

Similar to the derivation in single layer hole only device, introduction of factor ξ, will take into account the factor by which injected current exceeds current actuality carried by low mobility organic layer.

$$\phi_h \leq -kT \ln\left[\frac{\xi}{q v n_0} \times \varepsilon_0 \varepsilon_r \times \mu_p \times \frac{q}{kT} \times \frac{(V - V_{bi})^3}{d_2^3}\right] + \Delta E_V \qquad (4.3.2.4)$$

Fig 4.7 shows comparative trend followed in the variation of transition point w.r.t. to change in valence band discontinuity ΔE_v, for ξ=10. Figure shows that the trend predicted by Eq. (4.3.2.3) is in good agreement with the values obtained by numerical simulator. However the barrier heights at the contact given by Eq. (4.3.2.3) are an overestimation of values obtained with the help of simulator. This fact can be better justified in reference to Fig.4.2, which shows that the current value given by Eq. (4.3.2.1) exceeds total device

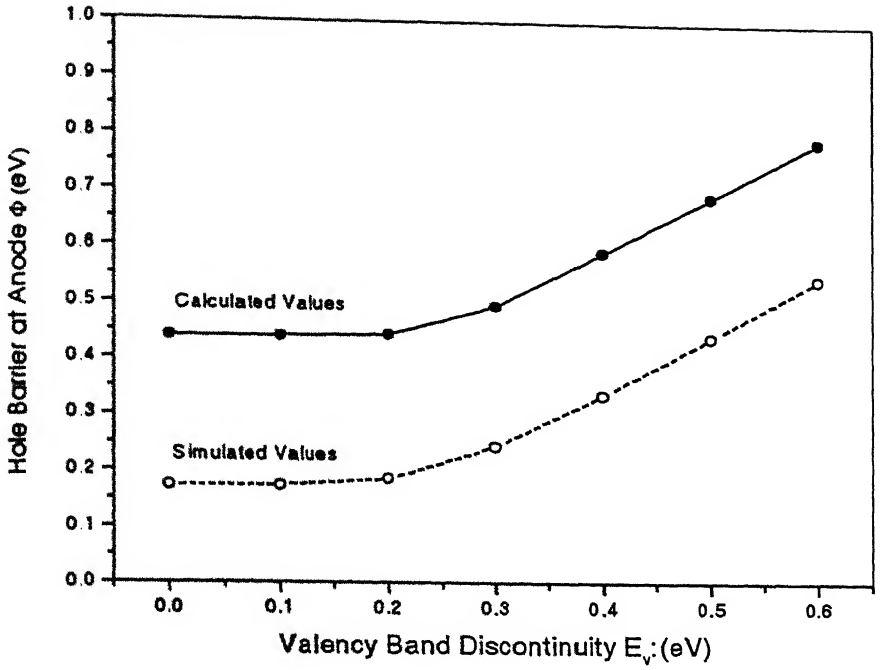

Fig.4.7 Shows variation in transition point from SCLC to contact limited regime as a function of valence-band discontinuity for a bilayer hole only device. Open circle denotes values obtained from the simulator and solid circles denotes the values obtained from Eq. (4.3.2.4) at 12V for ξ=10.The hole (electron) mobility in both the layers is 0.5×10^{-6}(0.5×10^{-8}) cm2/V-sec. The hole injection barrier at anode is 0.2eV.

current, by 2-9 orders of magnitude, depending on applied bias and energy barrier at the contact. It can also be seen that for the bilayer devices energy barrier ϕ_h, is greater than the energy barrier obtained for a single layer hole only device. In a bilayer device space charge is certainly enhanced because of the presence of barrier at the organic interface, and hence bulk dominated range is obtained for greater value of energy barrier at the contacts, than in case of single layer device. Also as the hole energy barrier at the interface increases, range for the bulk dominated conduction increases.

4.3.3.Analytical model: Bilayer device with bipolar injection:

Similarly analytical model for bilayer device under bipolar injection can be obtained with reference to current density equation in chapter.3 as:

$$J = \left(\frac{9}{8}\right)\mu_{n2}(\varepsilon_0\varepsilon_r)\frac{(V-V_{bi})^2}{d_2^{\,3}} \le \frac{1}{\xi}\times qvn_o \times \exp(-\phi_b / kT) \qquad (4.3.3.1)$$

$$\phi_b \le -kT\ln\left[\left(\frac{\xi}{qvn_o}\right)\times\left(\frac{9}{8}\right)\mu_{n2}(\varepsilon_o\varepsilon_r)\frac{(V-V_{bi})^2}{d_2^3}\right] \qquad (4.3.3.2)$$

Here n_0 can be equal to density of conjugated states for conduction band or valence-band depending on the electron (hole) injecting contact.Fig.4.8 shows the trend followed in transition point with change in barrier at interface. The calculated and simulated values follow similar trend with change in discontinuity at organic interface. Fact that the equation is obtained without any reference to barrier at the interface is reflected in nature of plot. The difference between the electron and hole barrier heights in simulated values is due to the difference in electron and hole mobility.

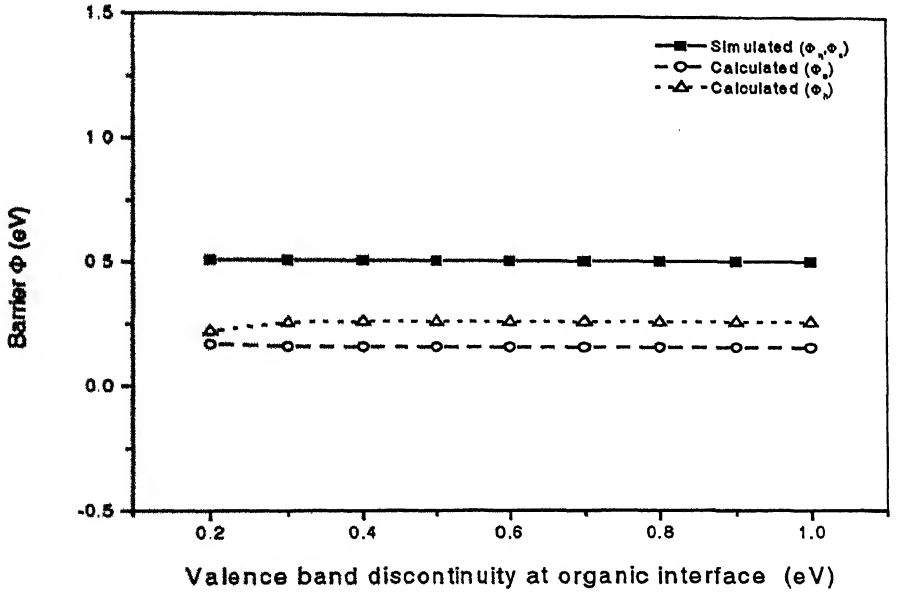

Fig.4.8 Shows variation in transition point from SCLC to contact limited regime as a function of valence-band discontinuity for a bilayer device under bipolar injection condition. Open symbols denotes values obtained from the simulator and solid circles denotes the values obtained from Eq. (4.3.3.2) at 12V for ξ=10.The hole (electron) mobility in both the layers is $0.5\times10^{-6}(0.5\times10^{-8})$ cm^2/V-sec.

Chapter5

Conclusions:

OLEDs are a relatively new type of device. The results of this work are aimed at gaining insight into fundamental issues of the device operation and to put more intuitive reasoning on firm theoretical basis under analytical framework. In the present work, analytical models are developed for bilayer devices in particular, which reveals the dependence of current, efficiency etc. on various device parameters.

In this effort, analytical models for bilayer hole only device have been developed. These models include 'valence-band' and mobility discontinuity effects. The analytical models adequately describe the current-voltage characteristics of the device in the forward as well as reverse direction. The developed model predicts that under forward bias condition current is interface barrier limited for larger barrier heights, and the dependence of current on both the voltage and thickness of hole blocking layer is identical. The model predicts current density from large to small hole barrier heights at the organic interface and is found to be valid for arbitrary values of hole barrier heights and mobility ratios. While under the reverse bias condition current is still found to be space charge limited with important effects of mobility ratio in the transport and blocking layer. The bilayer device under bipolar injection condition, with a variety of thicknesses and energy barriers at the organic interface has been studied.

The analytical model developed for bipolar bilayer device describes the current-voltage characteristics in the forward direction. Along with this, bilayer device structures under bipolar injection condition were aimed at studying recombination with change in the electron-level and hole-level offsets at the organic interface and gaining insight into fundamentals controlling recombination rate profile. It has been observed that best

recombination magnitude and profile is observed when the 'valence-band' offset $\Delta E_v = 0.6eV$ and 'conduction-band' offset, $\Delta E_c \geq 0.6eV$.

The analytical models are developed under the assumption of bulk-limited conduction. Elaborating upon this idea, the analytical expressions are developed to explore the injection conditions, when the developed models are likely to hold good. These analytical models define the range of energy barrier at the carrier injecting contact, both in single layer as well as in bilayer device structures, when the condition of bulk-limited transport in the device is satisfied. Analytical expressions are able to model the effect of band discontinuity in maintaining condition of bulk-limited conduction.

To summarize these *ab initio* analytical models can provide a substantial contribution to the study of current voltage characteristics and injection and transport processes involved. The developed models are parameter-free and does not rely on any specific physical or chemical mechanism of the device which makes them good candidate for ubiquitously explaining the observed behavior The validity of these developed models are investigated by the means of numerical simulation. A number of new insights have emerged from this study, and we emphasize the consequences of the properties thus discovered with respect to the functioning of OLED devices. In particular OLEDs can be designed and better understood with the aid of these analytical expressions. These models, however are not backed up by the experimental results.

However, in order to analytically describe current in bilayer devices certain simplifying assumptions were made. Thus applicability of these models in practical devices is a matter of these assumptions and can be reviewed. Further, refinement by removing these simplifying assumptions will ultimately lead to their practical applicability. Further refinement is possibly by considering trap filled cases and taking recombination into account. These models can be naturally extended to more structurally complex cases.

References

1. A. J. Campbell, D. D. C. Bradley, and D. G. Lidzey, J. Appl. Phys. **82,** 6326(1997).

2. B. K. Crone, P. S. Davids, I.H. Campbell, and D.L.Smith, J. Appl. Phys. **84,** 833(1998).

3. B. K. Crone, I. H. Campbell, P. S. Davids, and D. L. Smith, J. Appl. Phys. **86,** 5767(1999).

4. R. H. Friend, R. W. Gymer, A. B. Holmes *et. al.* Nature, **397,** 121(1999)

5. B. K. Crone, P. S. Davids, I.H. Campbell, and D.L.Smith, J. Appl. Phys. **87,** 1974(2000).

6. H. Bassler, Y. H. Tak, D. V. Khramtchenkov, V. R. Nikitenko, Synth. Metals, **91,** 173(1997).

7. D. V. Khramtchenkov, V. I. Arkhipov, and H.Bassler, J. Appl. Phys. **81,** 6954(1997).

8.Y. H. Tak and H. Bassler, J. Appl. Phys. **81,** 6963(1997).

9. P. S. Davids, I. H. Campbell, and D. L. Smith, J. Appl. Phys. **82,** 6319(1997).

10. I. D. Parker, J. Appl. Phys. **75,** 1656(1994).

11. P. S. Davids, Sh. M. Kogan, I. D. Parker, and D. L. Smith, Appl. Phys. Lett. **69,** 2270(1996).

12. I. H. Campbell, P. S. Davids, and D. L. Smith, Appl. Phys. Lett. **72,** 1863(1998).

13. J. Campbell Scott, Phillip J. Brock, Jesse R. Salem, Sergio Ramos, George G. Malliaras, Sue A. Carter, Luisa Bozano, Synth. Metals, **111-112,** 289(2000).

14. E. M. Conwell and m. W. Wu, Appl. Phys. Lett. **70,** 1867(1997).

15. S.M.Sze, *Physics of Semiconductor Devices*, 2nd Edition (Wiley New York, 1999).

16 ."Modeling and simulation of organic light emitting diode (OLED)", M.Tech. thesis by Flt. LT. CG. Narasimha Prasad. Jan,2002 IITK.

17. David W.Winston, SimWindows, Semiconductor Device Simulator, Version 1.5, 1999.

Appendix

SimWindows:

SimWindows is a semiconductor device simulation program originally developed at the Optoelectronics Computing Systems Center at the University of Colorado, Boulder. It handles a variety of optoelectronic devices by solving the semiconductor equations in one dimension. As a result, SimWindows assumes that all variables such as current, field and potential, etc. vary parallel to the flow of current but are uniform in the direction perpendicular to the current. Simulation tools help device designers determine how these various effects interact. The software extends many of the traditional electrical models, optical model and thermal models. These combinations of models can predict many aspects of optoelectronic devices that traditional simulation programs cannot. SimWindows provides a large degree of flexibility for the user to control and modify the models in SimWindows. The user can also add new models depending on the circumstances.

The modified material parameter files used for organic material-1 and organic material-2 are shown below:

Material parameter file:

#MEH_PPV
Organic Material-1
Alloy=Default
BAND_GAP Value=2.4
ELECTRON_AFFINITY Value=3
STATIC_PERMITIVITY Value=3
REFRACTIVE_INDEX Value=3.44
ABSORPTION Segments=4
start_e=0.0 end_e=1.1 value=0.0
start_e=1.1 end_e=2.5 model=power_absorption terms=6e3,0,0,1.1,2

start_e=2.5 end_e=3.2 value=6e3*(E-1.1)^2+8e4*(E-2.5)^2

start_e=3.2 end_e=100 value=6e3*(E-1.1)^2+8e4*(E-2.5)^2+1.26e6*(E-3.2)^0.5

THERMAL_CONDUCTIVITY Value=1.412

DERIV_THERMAL_CONDUCT Value=0

ELECTRON_MOBILITY Value=0.5e-8

HOLE_MOBILITY value=0.5E-6

ELECTRON_DOS_MASS Value=1.4e1

HOLE_DOS_MASS Value=1.4e1

ELECTRON_COND_MASS Value=0.26

HOLE_COND_MASS Value=. 386

ELECTRON_SHR_LIFETIME Value=1.0e-06

HOLE_SHR_LIFETIME Value=1.7e-06

ELECTRON_AUGER_COEFFICIENT Value=1.5e-31

QW_ELECTRON_AUGER_COEFFICIENT Value=0.0

HOLE_AUGER_COEFFICIENT Value=1.5e-31

QW_HOLE_AUGER_COEFFICIENT Value=0.00

RAD_RECOMB_CONST Value=3e-13

ELECTRON_ENERGY_LIFETIME Value=1.0e-8

HOLE_ENERGY_LIFETIME Value=1.0e-8

QW_RAD_RECOMB_CONST Value=0.0

ELECTRON_COLLISION_FACTOR Value=-0.5

HOLE_COLLISION_FACTOR Value=-0.5

#CN_PPV

Organic Material-2

Alloy=Default

BAND_GAP Value=3

ELECTRON_AFFINITY Value=3

STATIC_PERMITIVITY Value=3

REFRACTIVE_INDEX Value=3.44

ABSORPTION Segments=4

start_e=0.0 end_e=1.1 value=0.0

start_e=1.1 end_e=2.5 model=power_absorption terms=6e3,0,0,1.1,2

start_e=2.5 end_e=3.2 value=6e3*(E-1.1)^2+8e4*(E-2.5)^2

start_e=3.2 end_e=100 value=6e3*(E-1.1)^2+8e4*(E-2.5)^2+1.26e6*(E-3.2)^0.5

THERMAL_CONDUCTIVITY Value=1.412

DERIV_THERMAL_CONDUCT Value=0

ELECTRON_MOBILITY Value=0.5e-8

HOLE_MOBILITY value=0.5e-06

ELECTRON_DOS_MASS Value=1.4e1

HOLE_DOS_MASS Value=1.4e1

ELECTRON_COND_MASS Value=0.26

HOLE_COND_MASS Value=.386

ELECTRON_SHR_LIFETIME Value=1.e-70

HOLE_SHR_LIFETIME Value=1.e-7

ELECTRON_AUGER_COEFFICIENT Value=1.5e-31

QW_ELECTRON_AUGER_COEFFICIENT Value=0.0

HOLE_AUGER_COEFFICIENT Value=1.5e-31

QW_HOLE_AUGER_COEFFICIENT Value=0.0

RAD_RECOMB_CONST Value=3e-13

ELECTRON_ENERGY_LIFETIME Value=1.e-8

HOLE_ENERGY_LIFETIME Value=1.e-8

QW_RAD_RECOMB_CONST Value=0.0

ELECTRON_COLLISION_FACTOR Value=-0.5

HOLE_COLLISION_FACTOR Value=-0.5